NASA TN D-88

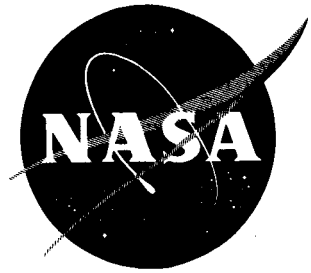

TECHNICAL NOTE

D-88

WIND-TUNNEL TESTS OF A SEMISPAN WING WITH A FAN ROTATING IN THE PLANE OF THE WING

By David H. Hickey and David R. Ellis

Ames Research Center
Moffett Field, Calif.

NATIONAL AERONAUTICS AND SPACE ADMINISTRATION

WASHINGTON

October 1959

NATIONAL AERONAUTICS AND SPACE ADMINISTRATION

TECHNICAL NOTE D-88

WIND-TUNNEL TESTS OF A SEMISPAN WING WITH A FAN ROTATING IN THE PLANE OF THE WING

By David H. Hickey and David R. Ellis

SUMMARY

An investigation was conducted to determine the aerodynamic characteristics of an aspect-ratio-4 semispan wing model with a fan-rotating in the plane of the wing. The effects of a ground plane, fan duct inlet and exit vanes, and a wing leading edge with increased camber and radius were obtained.

Three-component forces, air flow through the fan, wing static pressures, and power input to the electric motor, were measured. These data cover tip-speed ratios from 0 to 0.5.

The data indicate ground effect causes a significant loss in lift, duct inlet vanes improve aerodynamic characteristics and flow through the propeller disk, and duct exit vanes can be used to redirect the propeller flow for propulsion.

INTRODUCTION

Provision for VTOL or STOL capabilities by use of a direct lifting fan enclosed in a wing has been proposed. Reference 1 presents results from a preliminary two-dimensional investigation of this scheme. References 2 through 5 report results from other pertinent investigations.

The investigation reported in reference 1 revealed several problems inherent in this VTOL method. These were severe unfavorable ground effect, wing leading-edge separation from induced lift, and oscillating propeller blade loads due to the asymmetric disk loading. The investigation reported herein was conducted to study these problems under three-dimensional operation on a more realistic model. Accordingly, the characteristics of a 15-percent-thick, unswept, aspect-ratio-4, semispan wing with the propeller axis at $0.5\bar{c}$ have been studied. The aerodynamic characteristics of the model with a ground plane, increased radius and camber at the wing leading edge, and propeller duct inlet and exit vanes were determined. Power requirements were also measured.

This report contains data showing longitudinal characteristics, some fan wake total pressures and wing static pressures, and input power to the propeller drive motor.

NOTATION

A	aspect ratio, $\frac{b^2}{S}$
C_L	lift coefficient, $\frac{\text{lift}}{q_\infty S}$
C_D	drag coefficient, $\frac{\text{drag}}{q_\infty S}$
C_F	propeller force coefficient, $\frac{L_p}{q_\infty S}$
C_m	pitching-moment coefficient about $0.5\bar{c}$, $\frac{\text{pitching moment}}{q_\infty S\bar{c}}$
C_p	power coefficient, $\frac{\text{power}}{\rho n^3 D^5}$
C_T	thrust coefficient, $\frac{\text{total lift}}{\rho n^2 D^4}$
c	wing chord, ft
$\bar{c}$	mean aerodynamic chord, $\frac{2}{S}\int_0^{b/2} c^2 dy$, ft
D	diameter, ft
HP	fan drive motor power output, horsepower
L	lift, lb
LE	leading edge
n	rotational speed, rps

P	pressure coefficient, $\frac{p_l - p_\infty}{q_\infty}$
p	static pressure, lb/sq ft
p_t	total pressure, lb/sq ft
q	dynamic pressure, lb/sq ft
q_1	average zero forward speed $p_{t_w} - p_\infty$ streamwise, lb/sq ft
q_2	average zero forward speed $p_{t_w} - p_\infty$ perpendicular to the wing chord, lb/sq ft
Δq_1	difference between the average $p_{t_w} - p_\infty$ from downstream to upstream, lb/sq ft
Δq_2	difference between the average $p_{t_w} - p_\infty$ from outboard to inboard, lb/sq ft
R	propeller radius, ft
r	radius of propeller element, ft
S	wing area, sq ft
T	fan thrust, lb
V	velocity, ft/sec
W	weight, lb
x	distance from the airfoil leading edge, measured parallel to the chord line, ft
y	distance perpendicular to the plane of symmetry, ft
z	distance perpendicular to the wing chord plane, ft
α	angle of attack, deg
β	propeller element blade angle at 0.75R
β_l	propeller element blade angle, deg
η	fraction of wing semispan, $\frac{2y}{b}$
θ	propeller duct vane angle, deg

μ tip-speed ratio, $\frac{V_\infty}{2\pi Rn}$

ρ mass density of air, slugs/cu ft

Subscripts

av average

e duct exit

i duct inlet

in inboard

l local or lower

p propeller

rpm at the same propeller rpm

s static

u upper

w fan wake

x variable

∞ free stream

MODEL AND APPARATUS

Figure 1 presents photographs of the model as installed in the Ames 7- by 10-foot wind tunnel. Pertinent geometric details of the model are shown in figure 2. Both the fan and the wing were mounted on the wind-tunnel balance system in order to measure total force. When propeller thrust in the presence of the wing was obtained, the wing was isolated from the balance system so that only the propeller forces were measured. The location of the wing remained the same. A 7- by 8-foot plane was used to simulate the ground during the ground effect tests. This plane was isolated from the wind-tunnel scale system and could be adjusted to any distance from the model wing.

Wing

The semispan wing model had an aspect ratio of 4, a semispan area of 12.5 square feet, a taper ratio of 0.5, and 0° sweep of the 0.50c line. An NACA 16-015 airfoil section (ordinates in table I) was employed to give nearly equal fore and aft propeller duct length. Rotational axis of the fan was on the mean aerodynamic chord at 0.50$\bar{c}$. Four chordwise rows of static-pressure orifices were placed in the wing at 0.17, 0.44, 0.71, and 0.85 of the wing semispan. For some tests, material was added to the lower surface of the wing to increase the leading-edge radius from the basic 1.10-percent chord to 1.25-percent chord at the root and to 2.50-percent chord at the tip. The radius variation from root to tip was linear. Enlargement of the leading-edge radius increased camber an arbitrary amount. Unless otherwise specified, the data and discussion pertain to the unmodified wing.

Propeller and Wake Survey Apparatus

Blade-form characteristics of the propeller are shown in figure 3. The airfoil section (ordinates in table II) of the propeller was an NACA 16-309 on a 66-series mean line. An electric motor was used to drive the propeller. Clearance between the propeller tip and the duct was 0.006 propeller radius. Propeller rotation was such that the advancing blade was on the outboard side of the propeller disk. Only the propeller blade angle, β, could be changed. The propeller was not equipped with flapping or drag hinges. Eight total-pressure rakes (at 45° intervals) were mounted radially at the duct exit.

Propeller Duct

Details of the propeller duct configurations are shown in figure 4. Inlet radii of 5- and 10-percent diameter were tested. Unless otherwise specified, the results presented are for the 10-percent diameter inlet radius. A cascade of thirteen 2-inch chord vanes, chosen to permit complete closure of the inlet, was used on the duct inlet as an inflow guide. In addition, a cascade of fifteen 2-inch chord vanes was added at the duct exit to redirect the flow for forward thrust. An NACA 65-(10A10)10 airfoil section was employed for the eight upstream elements of the inlet cascade. For the last five vanes of the inlet cascade and all fifteen elements of the exit cascade, an NACA 65-010 section was used.

TEST AND METHODS

The majority of testing was done with the wing at 0° geometric angle of attack. Wind-tunnel dynamic pressure, q, was maintained constant and propeller speed varied. For the studies to show effect of α, data were obtained by maintaining q and propeller speed constant through the angle-of-attack range. Propeller speeds ranged from 0 to 8,000 rpm; wind-tunnel dynamic pressure from 0 to 9 psf. Some data were obtained with constant angle of attack and propeller speed and variable q.

Individual inlet vane angles were adjusted to give unseparated air flow on the vanes (according to tuft observations) at a given q and propeller speed. After attaining smooth flow, data were taken for a range of q and rpm. A schedule of configuration numbers as assigned to these vane angles is given in table III. Data were also obtained with the inlet cascade set at angles of 0°, 8°, 15°, 30°, and 45°. Exit vanes were tested at angles of 0°, 10°, 15°, 20°, and 30°.

In general, as lift, drag, and pitching-moment coefficient data were obtained, total-pressure surveys behind the propeller and static pressure distributions on the wing were recorded.

The electrical input to the propeller drive motor was measured, and the horsepower was calculated assuming an electrical efficiency of 90 percent.

CORRECTIONS TO THE DATA

At the higher propeller loadings as much as 10 percent of the wind-tunnel air flow went through the propeller duct. A correction should be applied to the data to account for the blockage effect of this wake and the propeller drive motor and struts; however, a valid correction is unknown. Although this may leave some of the data open to question, it probably does not invalidate general trends and comparisons. As blockage corrections are not known, the wind-tunnel boundary corrections are of little value and were not applied to the data.

No corrections were applied to the force data for the interference effects of the motor and motor support struts on the wing and propeller.

RESULTS AND DISCUSSION

The discussion of the propeller-in-wing results covers three major aerodynamic areas. The first of these corresponds to zero forward speed conditions, the second to forward flight conditions with the wing at zero

angle of attack and, finally, the effect of angle of attack under forward flight conditions. Power requirements in these areas are presented separately.

Characteristics at Zero Forward Speed

Basic model.- The variation of lift with propeller rpm was determined for the complete model and for the propeller only in position in the wing. The results, obtained only with a blade angle of 31°, are shown in figure 5. Lift of the propeller alone was about 60 percent of the combination.

Within the rpm range studied, the static lift (thrust) of either the complete model or propeller only can be approximated for each blade angle by a single value of C_T. These results are similar to those for a free propeller. The effect of blade angle on the value of C_T for the wing-propeller combination is shown in figure 6; above 31° blade angle the value of C_T decreased.

The data shown in figures 5 and 6 were obtained with a $0.1D_p$ duct inlet radius. To determine whether inlet radius would affect these characteristics, radii of both 0.05 and $0.1D_p$ were tested. No effect could be found.

Reference 1 showed that for a "two-dimensional" propeller-in-wing combination, a large and unfavorable ground effect existed; as the combination approached the ground, the lift became negative. The effect of ground proximity for the semispan combination is shown in figure 7 along with the results from reference 1. The effect is presented in terms of the lift measured with no ground plane.[1]

The results given in figure 7 show that the ground effect was smaller for the semispan model than for the two-dimensional model. Only when z/D_p was less than 1.0 was a loss in lift incurred. For both blade angles investigated, ground proximity caused a slight increase in lift between z/D_p values of 1 and 3, and an 18-percent lift loss at z/D_p of 1/2. A more thorough discussion of ground effect is given in reference 5.

An attempt was made to define a ground effect on pitching moment, but the small measured values and scatter in the data made this impossible.

Effect of vanes in the propeller duct.- The individual effects of inlet and exit cascades on the static lift of the model are presented in figure 8. The inlet vanes, when adjusted individually to give unseparated

[1]It was not possible to obtain a true "out-of-ground effect" lift because of the tunnel walls which were at a distance of $z/D_p = 3$ from the plane of the propeller.

air flow, gave no measurable change in static lift. These vane angles are listed in table III (Configuration 0). With all the inlet vanes alined with the propeller axis, lift was increased but, as will be shown later, power was also increased. Exit vanes alined with the propeller axis reduced lift and increased power slightly.

Characteristics at Forward Speed, 0° Angle of Attack

Basic model.- The absolute values of forces and pitching moment on the propeller and complete model are shown by the data in figures 9 and 10. These data are presented in absolute form so that static values can be compared with values under forward flight conditions. Data in figure 9 show the variation of characteristics with propeller rpm for several tunnel dynamic pressures, and in figure 10 the variation with tunnel dynamic pressure at several constant values of propeller rpm. These data indicate that, except at low speed and high propeller rpm, the complete model lift was larger with forward speed than statically. The loss in lift noted with low speed and high propeller rpm (see ref. 6) may be due to wing airflow separation or wind tunnel recirculation effects.

The ratios of lift at forward speed to that at zero forward speed (at constant values of rpm) are shown in figure 11 as a function of μ, the tip-speed ratio used in helicopter studies. The ratios are presented for the complete model lift and for the propeller-only lift in position in the wing. At the lowest value of μ studied, the propeller thrust was below the static thrust value; as μ was increased from this value the thrust increased until at the maximum μ reached, the thrust was 2.2 times as great as static thrust. This particular trend has been found in other studies of propellers near 90° angle of attack and rotors (see refs. 7 and 8).

Reasoning similar to that presented in reference 9 (jet flap theory) leads to a conclusion that the characteristics of the propeller-wing combination should be invariant, in coefficient form, if the ratio of propeller slipstream dynamic pressure to free-stream dynamic pressure (relative momentum) is held constant. Thus, if the results of figure 9 or 10 are presented in coefficient form as a function of a momentum coefficient ($C_F = T/q_\infty S$, where T is the propeller-only thrust in position in the wing), it would be expected that these data would be independent of test conditions (q and rpm) and propeller design. This momentum coefficient will be called the propeller force coefficient. The data in figure 9 are presented in figure 12 in incremental form as a function of propeller force coefficient. The lift increment due to the propeller only is, of course, exactly equal to the value of the force coefficient and is no evidence of correlation. The single curve representation possible in all other cases, however, does indicate that the ratio of these dynamic pressures defines the flow field of the combination. Use of the independent variable, C_F, rather than μ is preferable because it makes the data applicable to any fan design or blade angle.

Further support to the assertion that propeller-force coefficient defines the flow field is obtained from pressure measurements for the complete model test conditions of figure 9. In figure 13, minimum pressure coefficients at the wing leading edge and duct inlet radius are presented as a function of propeller force coefficient. The data, obtained at three forward speeds, form a single curve. The magnitude of these minimum pressures and the consideration of the probable adverse pressure gradients associated with such pressures indicate that it is possible for the propeller to induce flow separation on the wing.

With forward flight conditions (fig. 12), the fan lift is about 40 percent of the total lift except at very low values of propeller force coefficient. The drag of the fan only, caused by redirection of the free-stream air, is also about 40 percent of the total drag.[2] An effort was made to predict complete model drag. Propeller drag was computed, based on the method of reference 6, from the deduced average exit angle (discussed later). Induced drag was calculated as $(\text{induced lift})^2/\pi A$. The sums of these two component drags is presented in figure 14 along with the measured drag. Agreement was fair.

The fan moment (fig. 12) becomes increasingly negative with increasing propeller force coefficient although the total moment becomes increasingly positive.

Data similar to those in figure 12 were obtained with a 5-percent duct inlet radius. No difference in the test results due to changing duct inlet radius was measured.

Effect of inlet vanes.- Total pressure surveys made just below the fan during the subject investigation (fig. 15) showed a considerable amount of distortion of the flow through the propeller. The ordinates in figure 15 present the difference in wake dynamic pressures at several locations on the propeller disk.

Inlet guide vanes were studied in an effort to reduce this distortion. Several combinations of individual vane settings were used, each one experimentally determined to eliminate flow separation on all the vanes for one particular propeller force coefficient. These values (called design points) are indicated in figure 15. The chordwise variation in vane angle for each of the four arrangements is given in table III. It is clear from figure 15 that the inlet vanes make a sizable reduction in the nonuniformity of the propeller flow near the design point, and, as a consequence, a reduction in the oscillating stresses in the blade would be expected.

---

[2] A question can arise here regarding interference effects due to the exposed motor and support on drag and moment. The correlation of propeller drag and moment with C_F is taken to indicate that the interference effects did not alter appreciably or were, themselves, a function of C_F.

The incremental changes in lift, drag, and moment with propeller force coefficient are shown in figure 16[3] for several vane angle settings and for no vanes. For the data in figure 16(a), the vanes were individually adjusted (as in fig. 15); in figure 16(b), all the vanes were set at equal angles. Figure 16(a) shows that proper vane adjustment will give a slight increase in lift accompanied by an increase in drag compared to the corresponding no-vane value; where lift is lost, drag is reduced. Air-flow separation on some of the vanes when all vanes were set at equal angles (fig. 16(b)) caused a loss in lift for all vane settings. Drag increased for most. It is concluded that if vanes are used, it will be necessary to have each vane individually rather than uniformly scheduled with forward speed if a performance gain rather than a loss is to be possible.

Effect of duct exit vanes.- The characteristics of the model were determined with exit vanes redirecting the propeller slipstream rearward to provide a propulsive force. The results in figure 17 show that it was possible to nullify completely the model drag, thus indicating that exit vanes could be used for a net propulsive force in at least some portions of the speed range. This propulsive force was obtained with only a small reduction in lift or change in pitching moment.

The results in figure 17 also give an indication of the average angularity of flow through the fan at forward speeds. For example, at a propeller force coefficient less than 0.65 the 20° vane setting increased drag, indicating the fan thrust was being directed more vertically by the vanes; above 0.65 the drag was decreased, indicating the vanes added a thrust component to the propeller flow. An estimated variation of exit angle with propeller force coefficient is shown in figure 18. This angle is only an average since at any setting some separation was evident somewhere on the vanes. Figure 19 shows the calculated and measured variation of drag increment with propeller force coefficient for a 30° vane deflection. The comparison of the data indicates some induced horizontal force exists as well as the direct force due to redirecting the fan slipstream.

---

[3]All of the data of figure 16 are plotted versus the factor C_F. It must be recognized that this factor was determined experimentally only for the vanes-out case; the inclusion of vanes would, of course, vary L_p for equal values of β, rpm, and q. It has been considered here that the change in C_F for a given set of operating conditions would not be sufficient to obscure the effects of vanes so that the relation between C_F and q and rpm determined for the vanes-out case has been assumed to hold for all vane arrangements.

Characteristics at Forward Speed, Variable Angle of Attack

The basic longitudinal characteristics of the wing at various angles of attack with the propeller and motor removed from the wind tunnel are shown in figure 20 for four duct conditions: inlet only closed, exit only closed, both inlet and exit closed, and both inlet and exit open. The data show that from both a lift and drag standpoint, it is undesirable to have either inlet open or inlet and exit open. With only the exit open there was an unexpected increase in maximum lift as well as the expected increase in drag. The existence of this phenomenon was verified by repeated tests. No explanation can be offered other than the conjecture that flow in and out of the cavity effected a camber change or simulated a lower surface flap.

The characteristics of the model in pitch for several values of propeller force coefficients are shown in figure 21. Over the angle range tested the lift increment due to propeller operation did not change for the three lower force coefficients. The stability parameter dC_m/dC_L was approximately 0.20 for all cases. Although propeller operation increased $C_{L_{max}}$, the angle for $C_{L_{max}}$ was decreased as propeller force coefficient was increased. Pressure distribution and tuft studies showed that $C_{L_{max}}$ was fixed by leading-edge separation starting in the region in front of the propeller area.

A leading edge with increased radius and camber was installed on the model in an attempt to alleviate the leading-edge separation. The results (fig. 22) show that $C_{L_{max}}$ and the angle for $C_{L_{max}}$ was increased (13° at the highest value of C_F) by the modification. Tuft and pressure distribution studies indicated that $C_{L_{max}}$ then was limited by trailing-edge separation. Below the angle for $C_{L_{max}}$ with the normal leading edge, the modified leading edge did not affect the characteristics. No significant change in lift-curve slope, stability, or drag rise accompanied the leading-edge change.

Propeller Power Characteristics

These power data are derived from the measured electrical input to the propeller drive motor. It was assumed the electrical efficiency of the motor was a constant 90 percent.

Variation of power with propeller rpm for static test conditions.- It should be realized that, in general, these data can be expressed as a single value of power coefficient ($C_p \cong 0.59$). Scatter in the data and slight variations in C_p make it necessary to present these data as a function of rpm to establish the trends.

Figure 23 contains data showing the effect of inlet vanes and exit vanes on static propeller power requirements. The addition of inlet vanes individually adjusted (as discussed before) caused a slight increase of input propeller power. With all inlet vanes alined parallel to the propeller axis, a larger increase in power due to vanes was measured (with an increase in lift; see fig. 8). Exit vanes increased power (with a decrease in lift).

Variation of power with propeller force coefficient at 0° angle of attack.- Figure 24 presents the ratio of powers required at some airspeed to the power required with static test conditions for the same propeller rpm. These data, for $\beta = 31^{\circ}$, give a single line representation when plotted versus propeller force coefficient. The effect of inlet vanes on power is also shown. At small force coefficients, inlet vanes reduced power; above a force coefficient of 0.75, the inlet vane configurations tested increased power.

Consideration of the foregoing power ratio is only a partial index of performance, however, as the propulsion power must also be considered. The sum of lifting horsepower and propulsion horsepower required for level flight can be expressed as

$$HP = n_s^3\left(K_1 \frac{HP}{HP_s} + K_2 \frac{C_D}{C_L^{3/2}}\right)$$

where K_1 is HP_s/n_s^3, and K_2 is $K_3^{3/2}(2/\rho)^{1/2}/550S^{1/2}$. The value K_3 is defined as L_s/n_s^2 or, when $L_s = W$, $K_3 = W/n^2$. For this model, $K_1 = 3.2\times10^{-5}$, $K_2 = 1.43\times10^{-5}$, and $K_3 = 9.7\times10^{-3}$. For a given wing loading, the parenthetical expression in the above equation is an index of total power required for level flight. This index, obtained from data with and without inlet vanes, is shown as a function of propeller force coefficient in figure 25. For this model, inlet vanes reduced power required for level flight below a force coefficient of 0.8; above this value, inlet vanes increased power.

The general effect of exit vanes as shown by the data in figure 26 was an increase in the power ratio above a propeller force coefficient of 0.25.

Variation of power with angle of attack at a constant tip-speed ratio.- A great deal of scatter in the data was encountered because of the small power changes and difficulty in keeping test conditions constant with angle of attack. The power requirements for the data in figures 20 and 21 are plotted versus angle of attack in figure 27, as the ratio $(C_L - C_{L_{\alpha=0}})/(HP - HP_{\alpha=0})$. Most of the data falls between 0.6 and 1.2. This gives a rough indication of power changes with angle of attack.

CONCLUSIONS

1. Ground effect was less for the semispan model tested than that reported in NACA RM A57F03 for a two-dimensional wing, but still reduced static lift 18 percent when the ground plane was one-half of the propeller diameter from the wing.

2. Duct inlet vanes improved the over-all performance of the model at moderate propeller loadings. Asymmetric loads on the propeller were reduced with inlet vanes. Installation of the inlet vanes caused no loss in static lift and only a slight increase in power as long as the vane angles were properly adjusted.

3. Duct exit vanes can probably be used to provide thrust for forward flight. These vanes reduced static lift and increased power slightly.

4. Increasing leading-edge radius and camber greatly increased the maximum lift coefficient and the angle of attack for maximum lift.

Ames Research Center
National Aeronautics and Space Administration
Moffett Field, Calif., July 7, 1959

REFERENCES

1. Hickey, David H.: Preliminary Investigation of the Characteristics of a Two-Dimensional Wing and Propeller With the Propeller Plane of Rotation in the Wing-Chord Plane. NACA RM A57F03, 1957.

2. Ham, Norman D., and Moser, Herbert H.: Preliminary Investigation of a Ducted Fan in Lifting Flight. Jour. Amer. Helicopter Soc., July 1958.

3. Stepniewski, W. Z.: Vertol's Work in Ducted Fans. M.I.T. Ducted Fan Symposium, Dec. 4-6, 1959.

4. Sacks, Alvin H.: The Flying Platform as a Research Vehicle for Ducted Propellers. I.A.S. Preprint 832, Jan. 1958.

5. Spreeman, Kenneth P., and Sherman, Irving R.: Effects of Ground Proximity on the Thrust of a Simple Downward-Directed Jet Beneath a Flat Surface. NACA TN 4407, 1958.

6. Wardlaw, R. L., and Templin, R. J.: Preliminary Wind Tunnel Tests of a Lifting Fan in a Two-Dimensional Aerofoil. Canada, Natl. Aero. Est. Lab. Rep. LR-207, 1957.

7. McLemore, H. Clyde, and Cannon, Michael D.: Aerodynamic Investigation of a Four-Blade Propeller Operating Through an Angle-of-Attack Range From 0° to 180°. NACA TN 3228, 1954.

8. Owen, T. B., Fail, R., and Eyre, R. C. W.: Wind Tunnel Tests on a 6 Ft Diameter Helicopter Rotor. British A.R.C. CP 216, (Rep. 17,791), 1955.

9. Poisson-Quinton, Ph., and Jousserandot, P., (G. Boehler, trans.): High Lift and Control of Airplanes by Control of Circulation. Presented at Association Technique Maritime et Aeronautique, July 1955. French, Office National d'Etudes et de Recherches Aeronautiques. (Also available as Eng. Study No. 186, Univ. of Wichita, translated by H. B. Helmbold, Aug. 1955).

TABLE I.- ORDINATES OF THE NACA 16-015 AIRFOIL SECTION

x/c	z/c	x/c	z/c
0	0	0.40	0.07318
.0125	.01615	.50	.0750
.025	.02257	.60	.07293
.050	.03137	.70	.06587
.075	.03790	.80	.05248
.10	.04322	.90	.03147
.15	.05168	.95	.01768
.20	.05830	1.00	.0015
.30	.06772		
Leading-edge radius: 0.011c			

TABLE II.- ORDINATES OF THE NACA 16-309 AIRFOIL SECTION

x/c	z_u/c	z_l/c	x/c	z_u/c	z_l/c
0	0	0	0.40	0.06167	0.02615
.0125	.01066	.00872	.50	.06605	.02395
.025	.01548	.01160	.60	.06676	.02076
.050	.02260	.01504	.70	.06322	.01582
.075	.02879	.01719	.80	.05389	.00909
.10	.03317	.01869	.90	.03664	.00112
.15	.04137	.02065	.95	.02097	.00025
.20	.04813	.02183	1.00	.00090	.00090
.30	.05624	.02502			

TABLE III.- FAN-DUCT INLET VANE ANGLES

Vane no.	Configuration number				
	0	1	2	3	4
	θ_i, deg				
1	28	61	48	45	45
2	21	54	41	37	37
3	16	47	36	28	28
4	12	45	33	19	19
5	9	45	32	16	11
6	6	45	29	16	6
7	2	45	27	16	6
8	-3	41	26	15	7
9	-4	41	32	23	9
10	-9	41	34	21	4
11	-15	45	34	19	-1
12	-23	50	37	19	-4
13	-31	55	38	16	-8

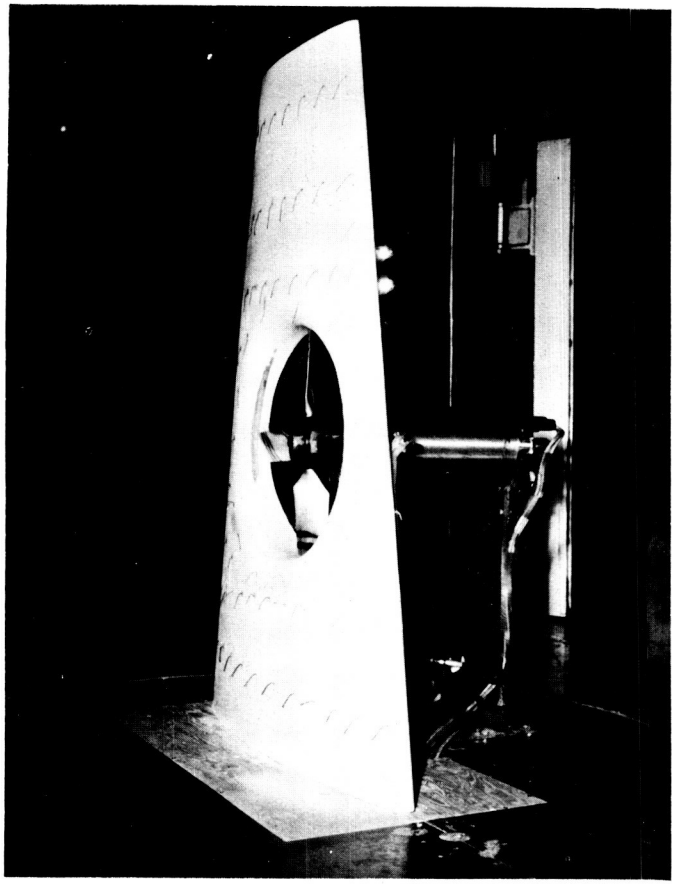

A-23992

(a) Upper surface from upstream.

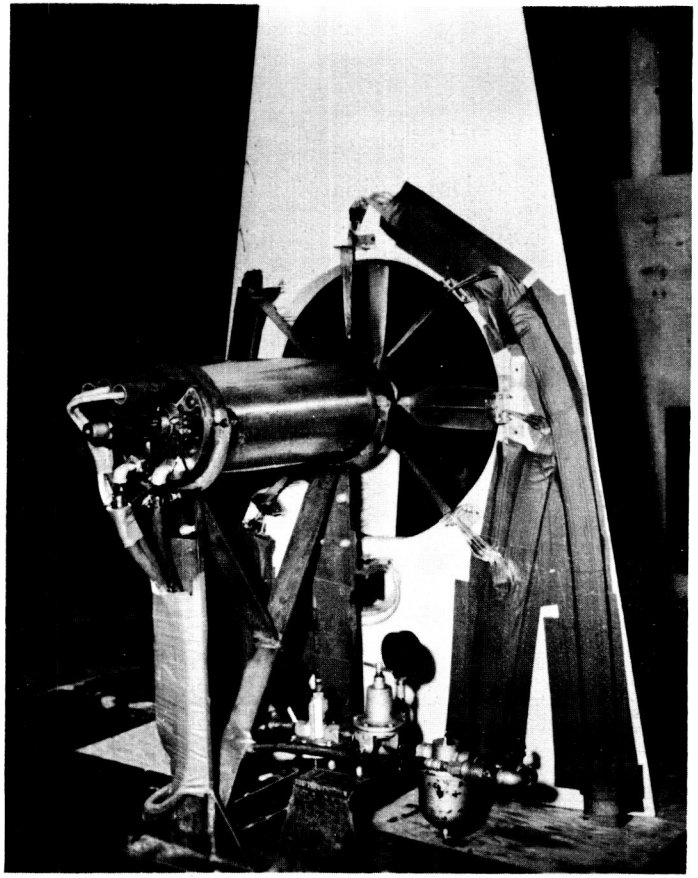

A-23994

(b) Lower surface from downstream.

Figure 1.- Views of the model as mounted in the Ames 7- by 10-foot wind tunnel.

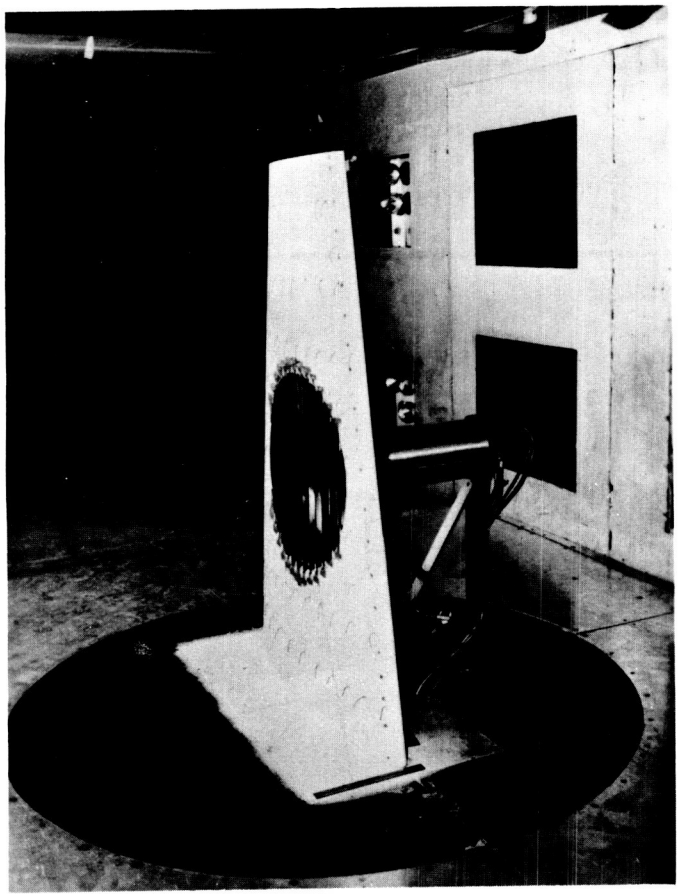

A-24092

(c) With inlet vanes.

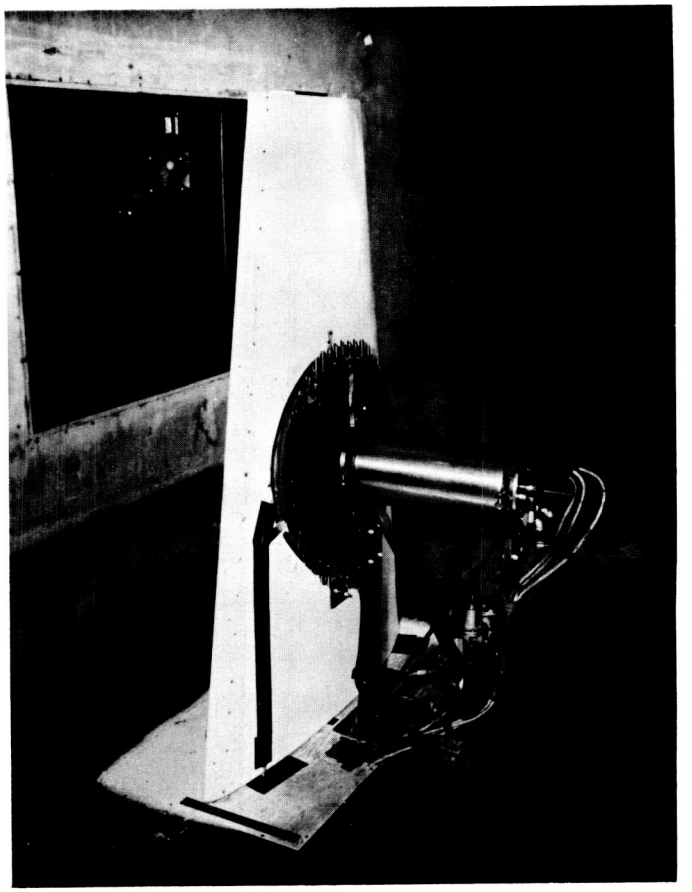

A-24094

(d) With exit vanes.

Figure 1.- Concluded.

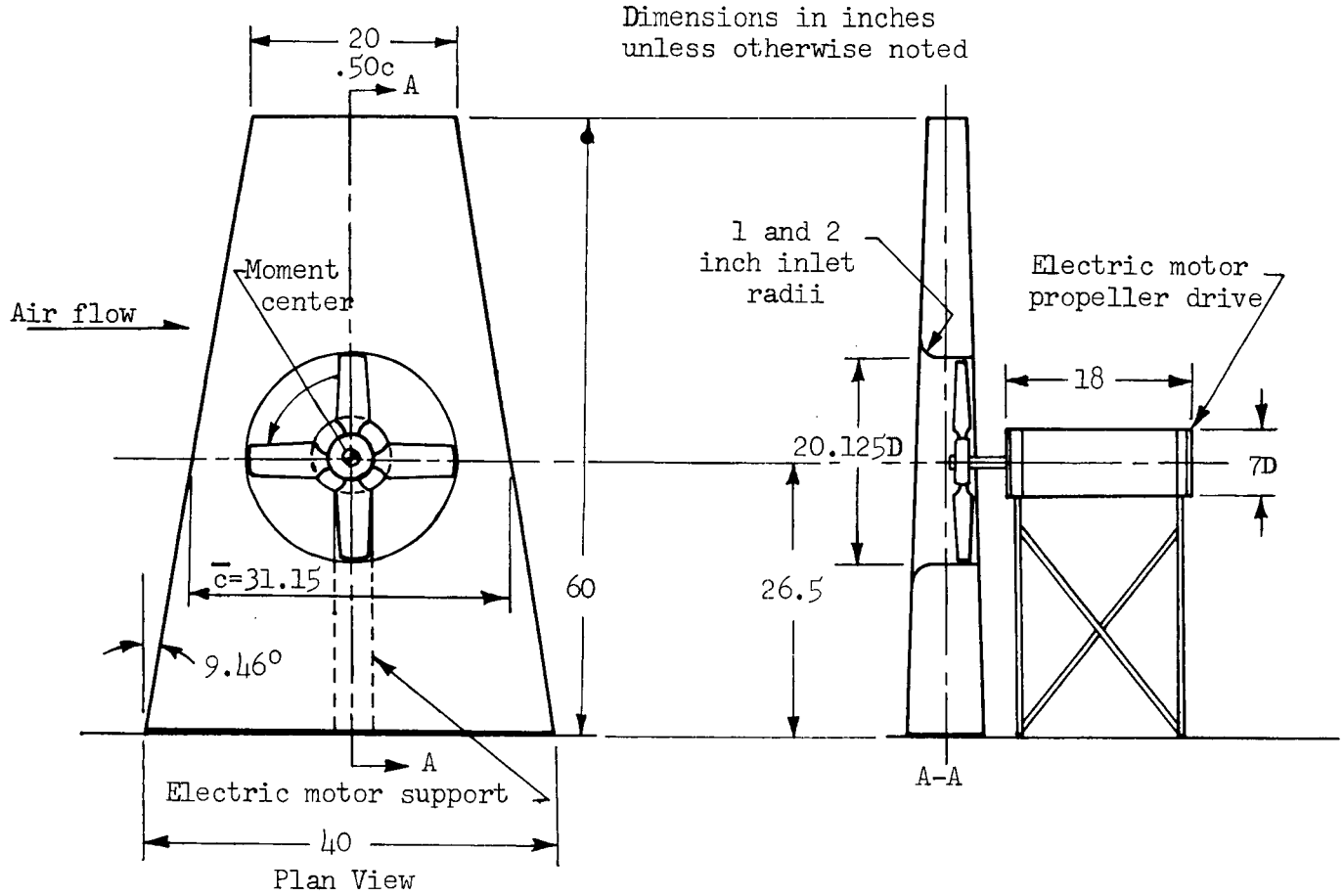

Figure 2.- Geometric characteristics of the model.

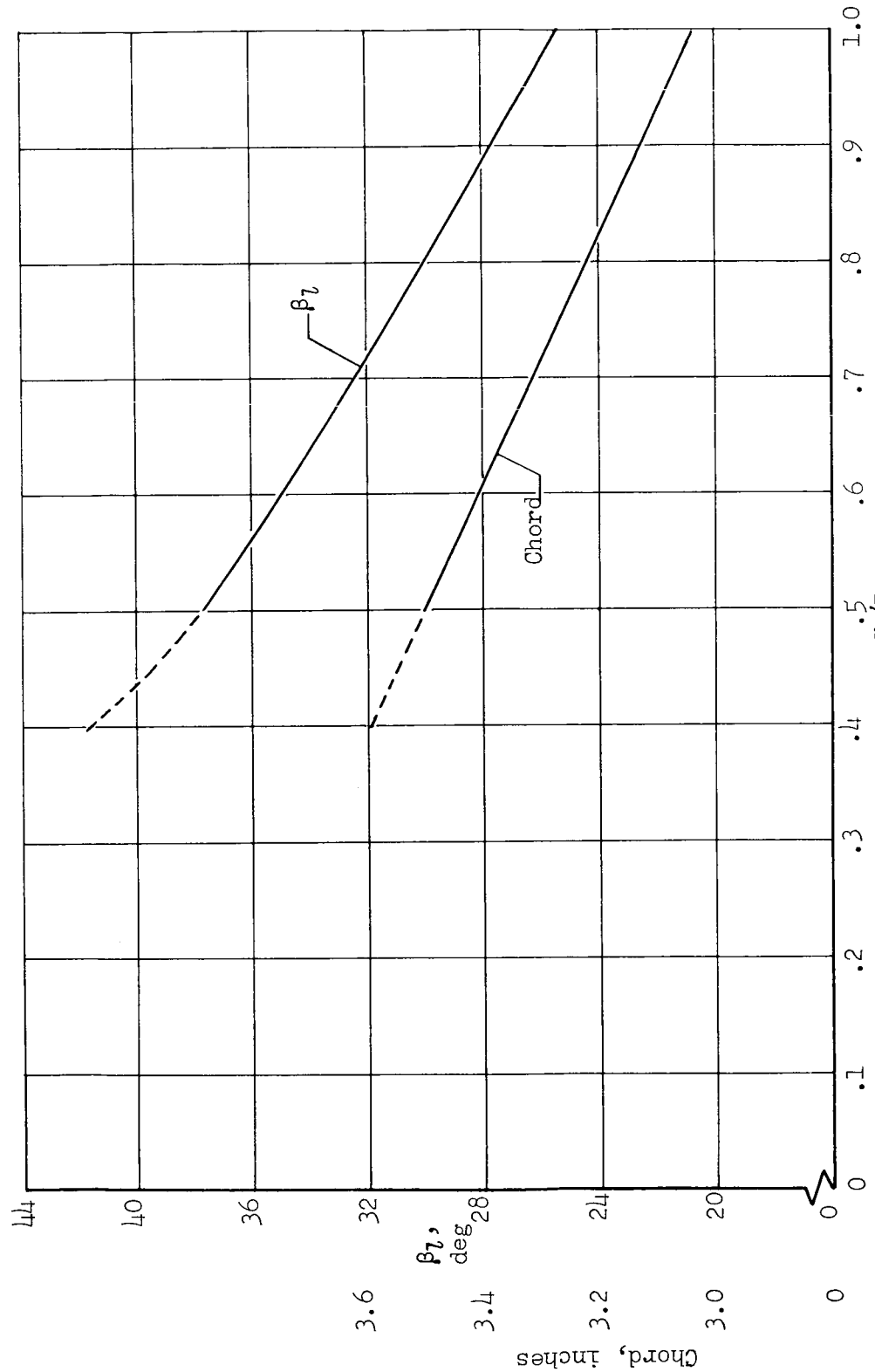

Figure 3.- Blade form curve of the propeller. The β shown was used for most of the testing.

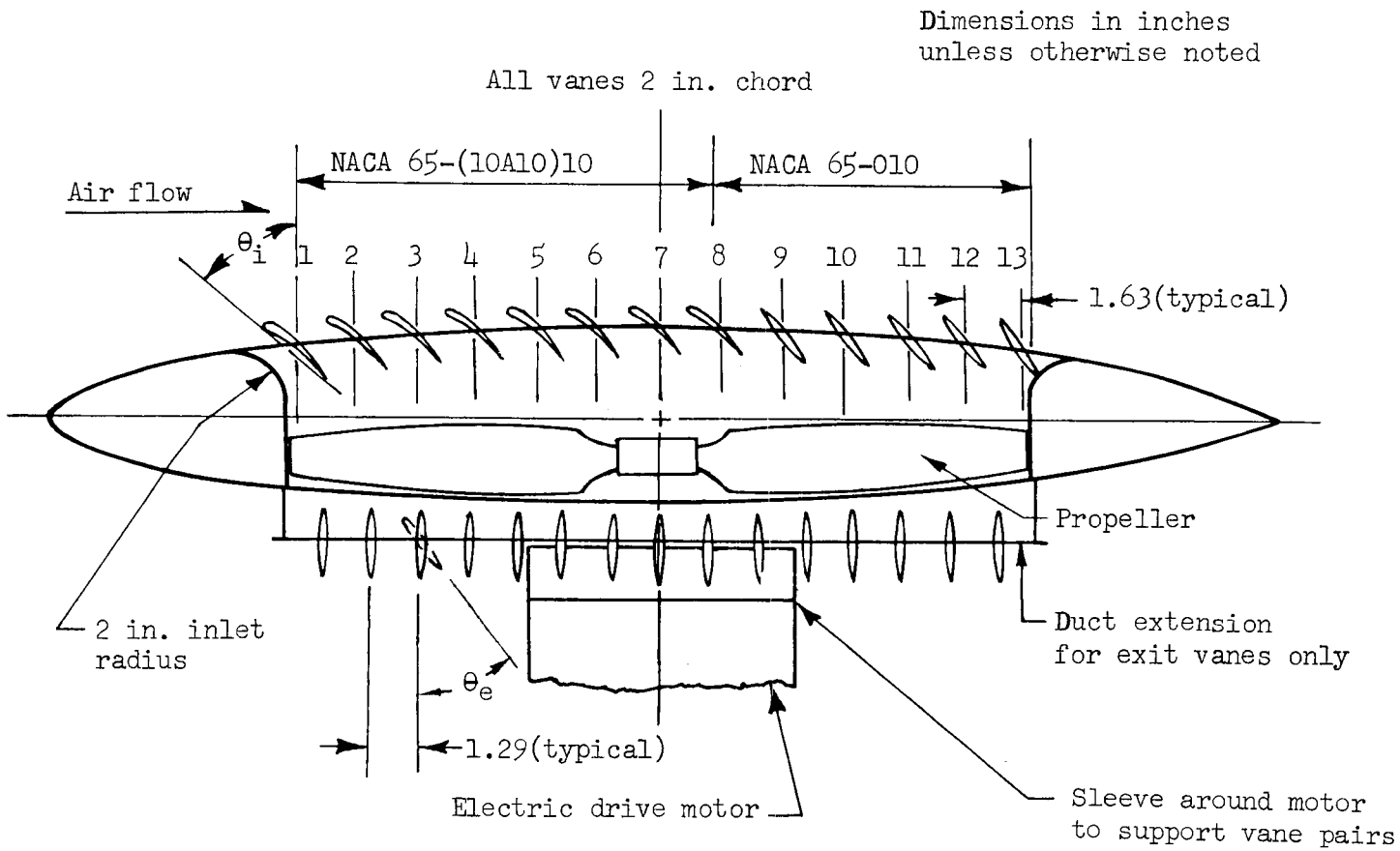

Figure 4.- Details of the inlet and exit vane configuration.

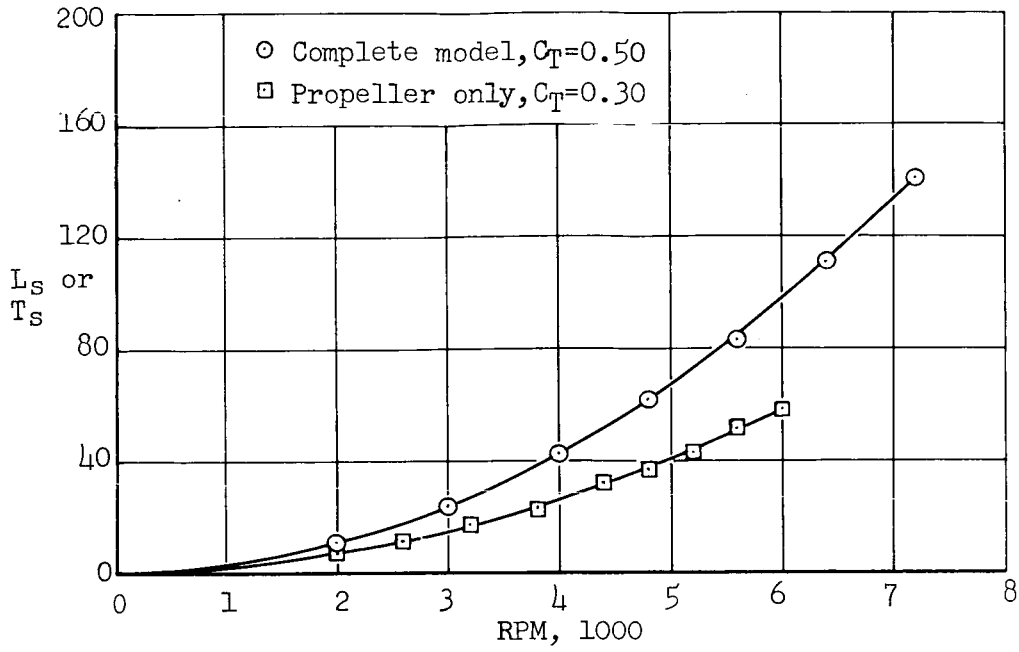

Figure 5.- Variation of static lift with propeller rpm; $\alpha = 0^\circ$, $\beta = 31^\circ$.

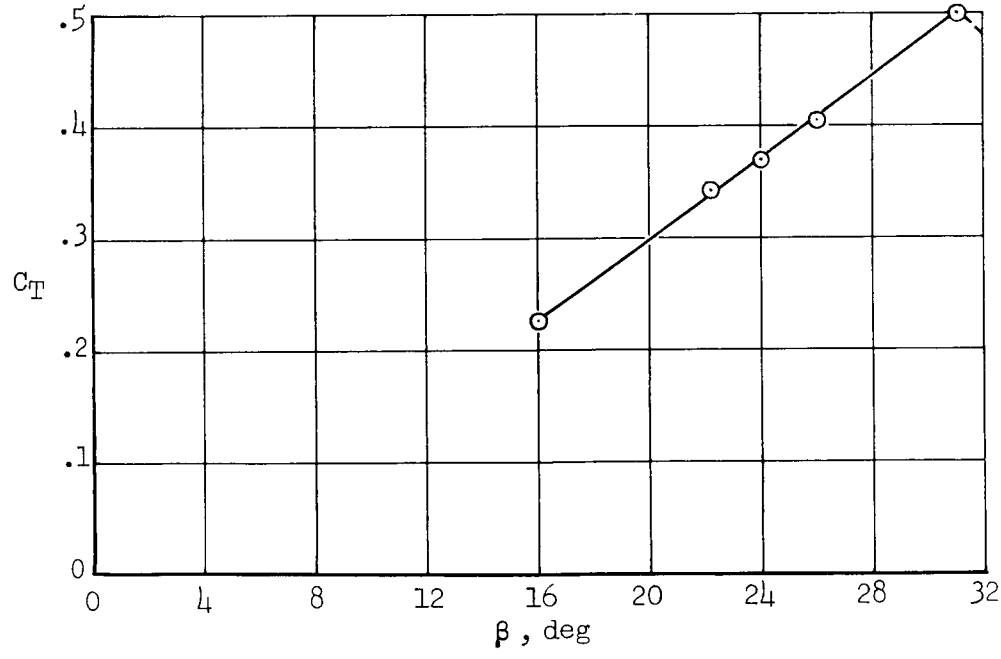

Figure 6.- Variation of static thrust coefficient of the complete model with blade angle; $\alpha = 0^\circ$.

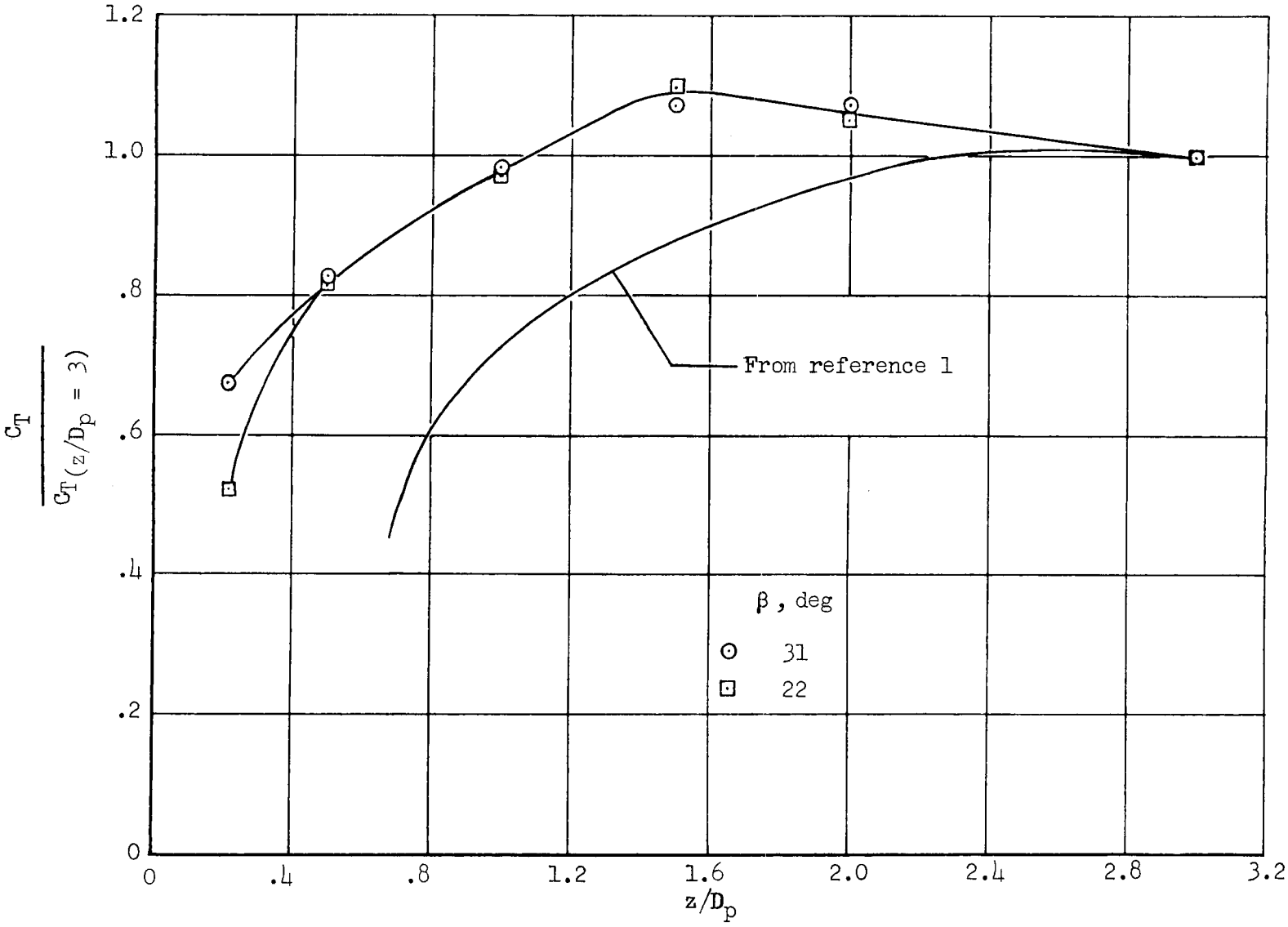

Figure 7.- The effect of ground proximity on static lift of the complete model; $\alpha = 0^\circ$.

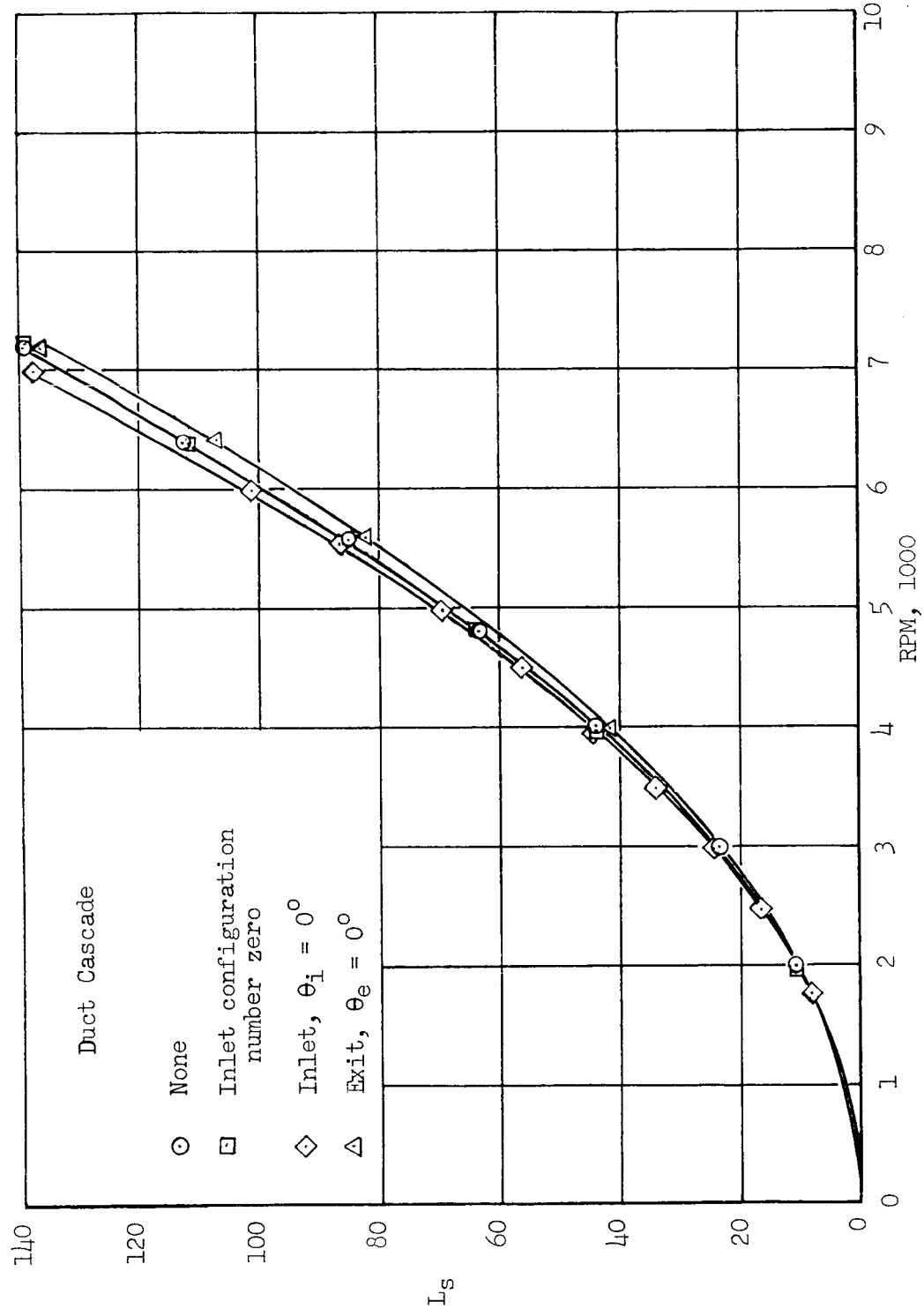

Figure 8.- The effect of duct inlet and exit vanes on the static lift of the complete model; $\alpha = 0°$, $\beta = 31°$.

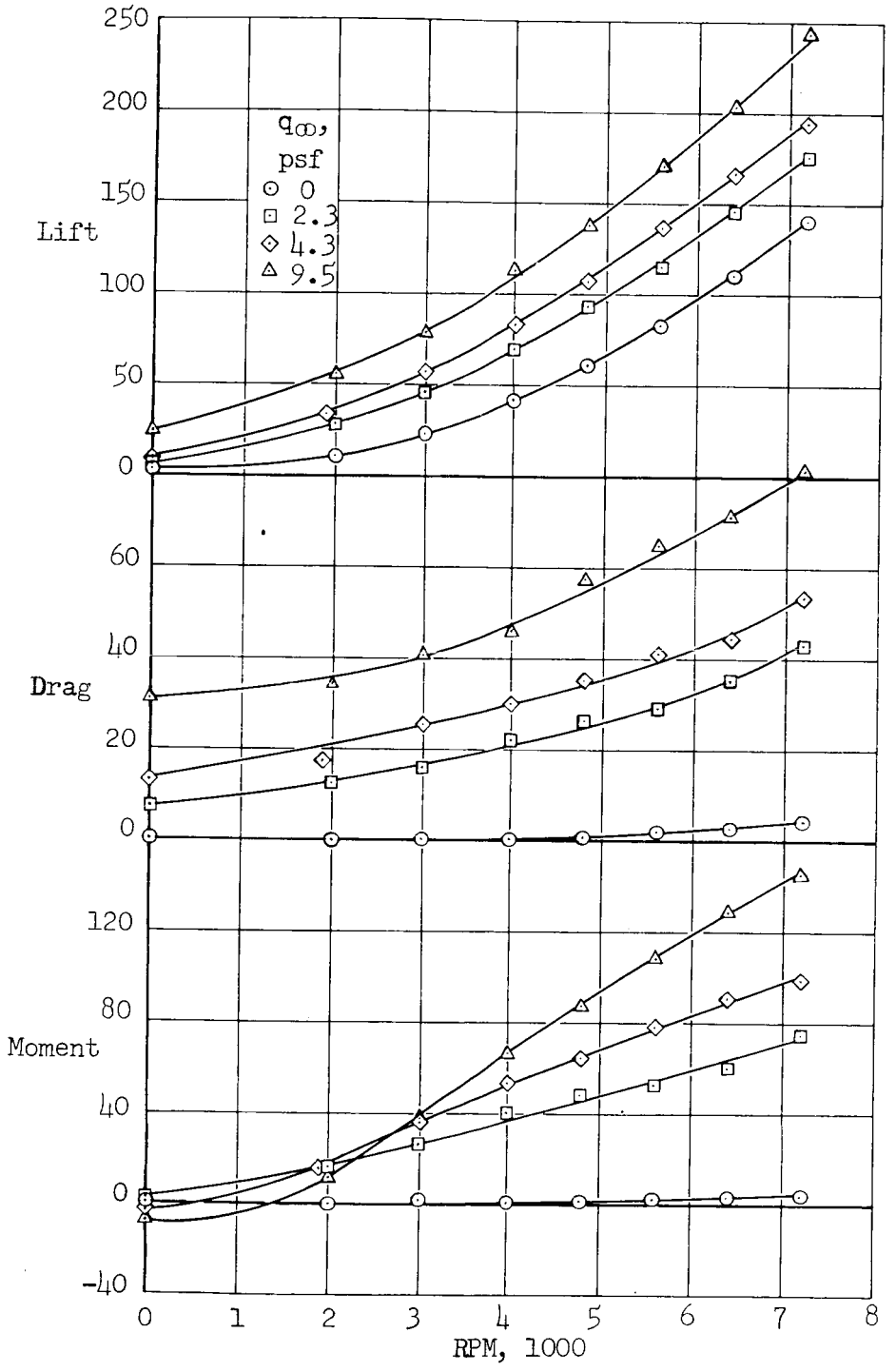

(a) Complete model.

Figure 9.- Variation of lift, drag, and pitching moment with propeller rpm; $\alpha = 0^\circ$, $\beta = 31^\circ$.

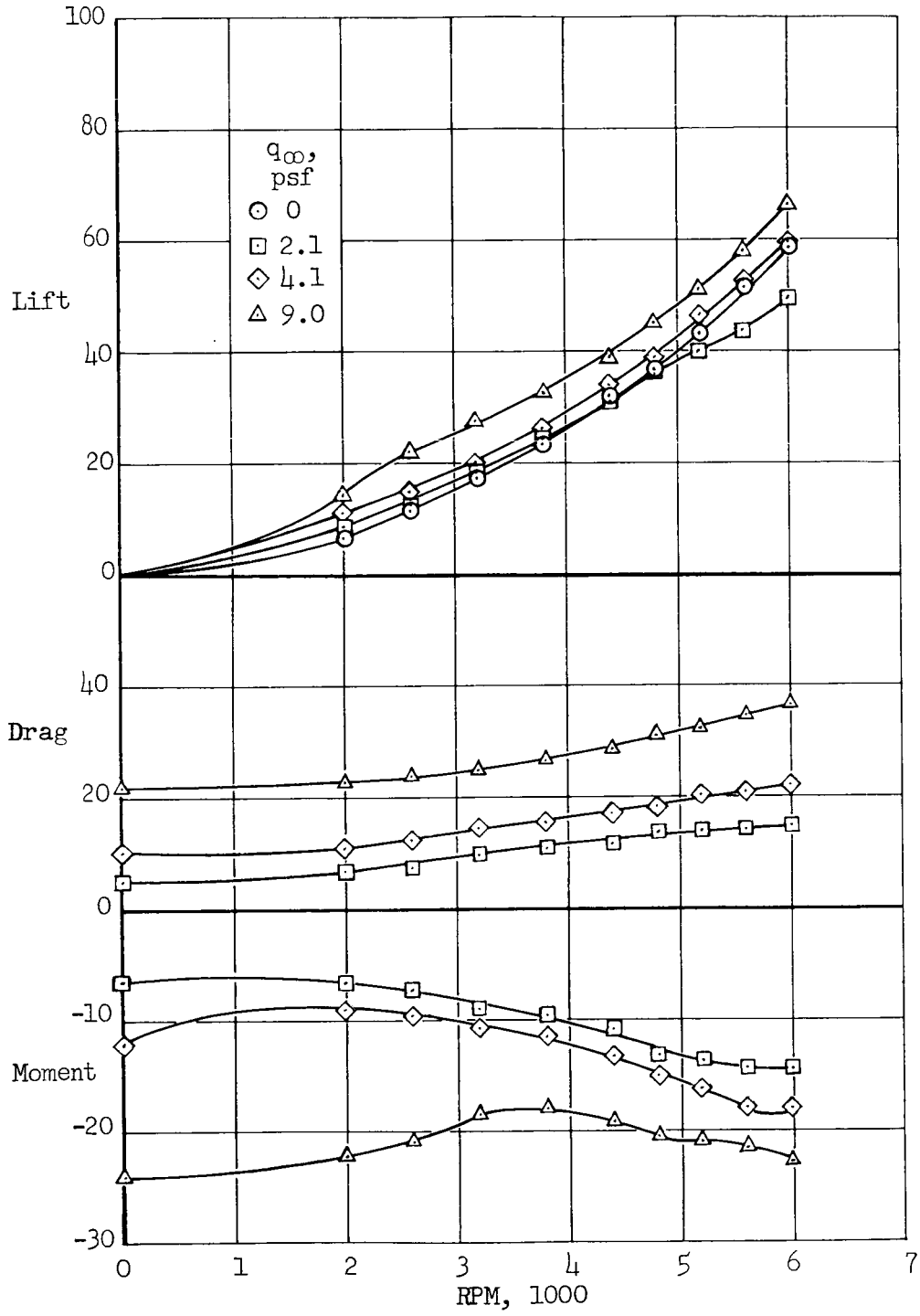

(b) Propeller only.

Figure 9.- Concluded.

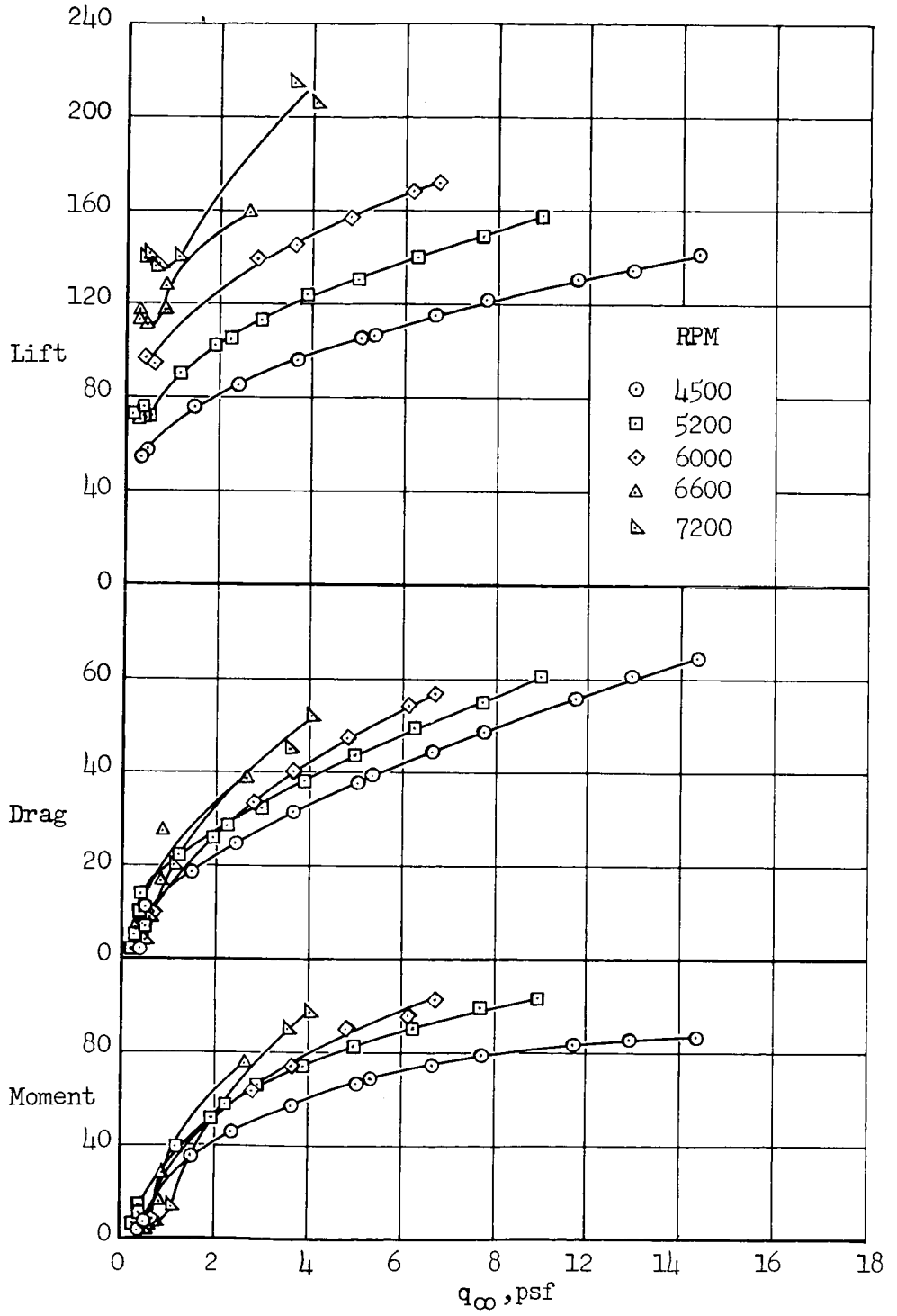

Figure 10.- Variation of lift, drag, and pitching moment with wind tunnel dynamic pressure for the complete model; $\alpha = 0^\circ$, $\beta = 31^\circ$.

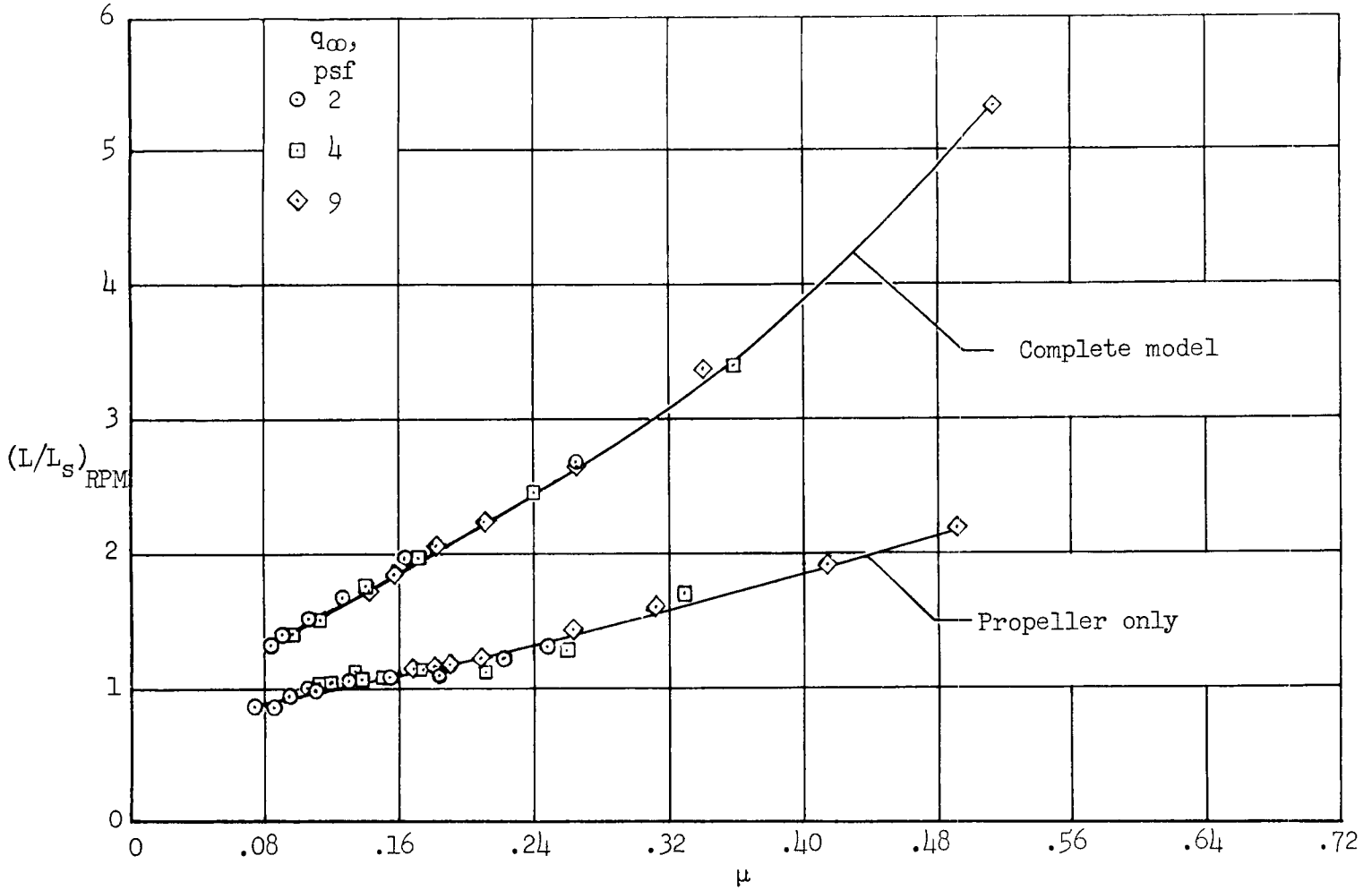

Figure 11.- The ratio of lift with forward speed to static lift for the same propeller rpm; $\alpha = 0^\circ$, $\beta = 31^\circ$.

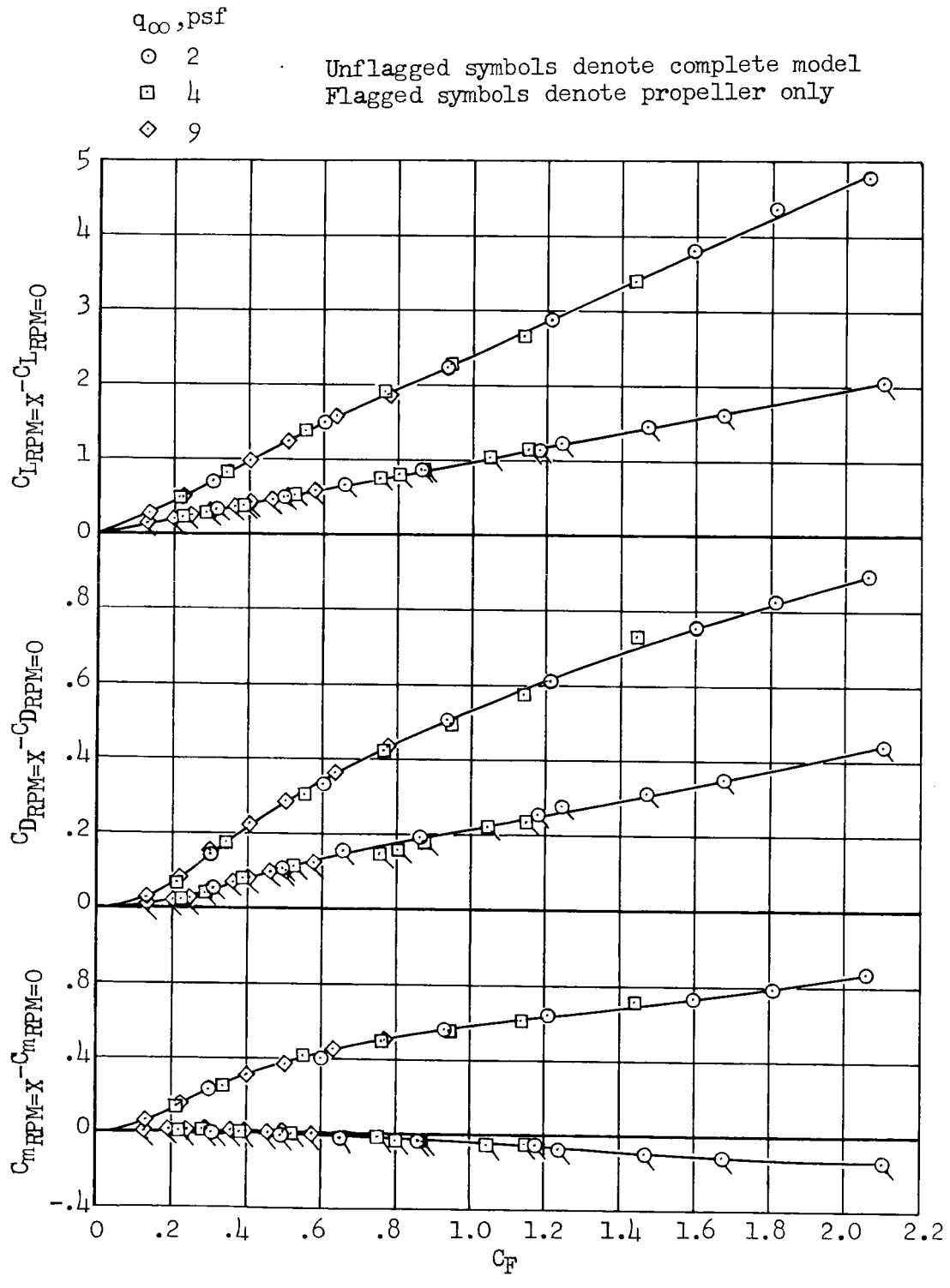

Figure 12.- Variation of incremental force and moment coefficients with propeller loading; $\alpha = 0^\circ$, $\beta = 31^\circ$.

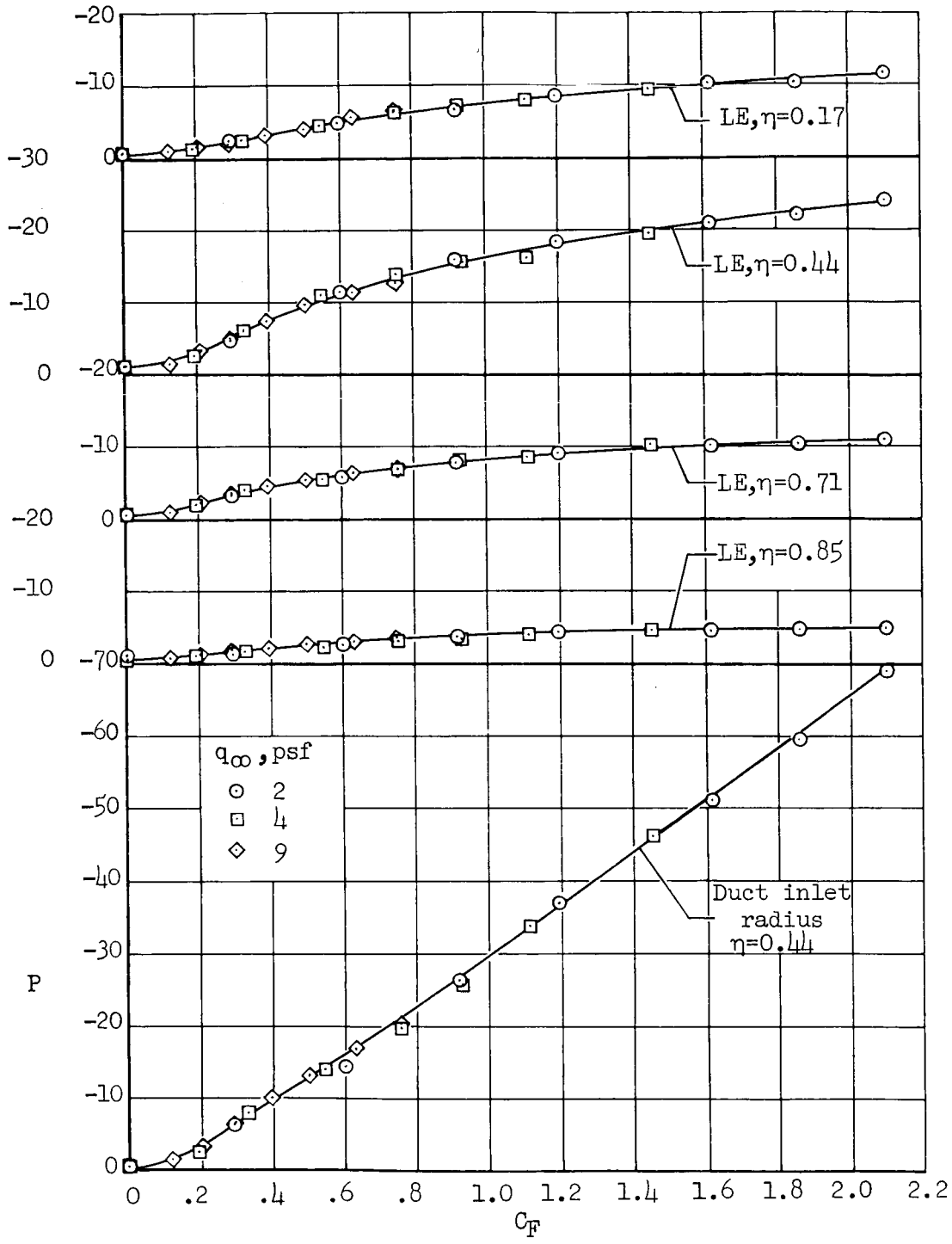

Figure 13.- Effect of propeller force coefficient on wing surface pressure coefficients; $\alpha = 0^{\circ}$, $\beta = 31^{\circ}$.

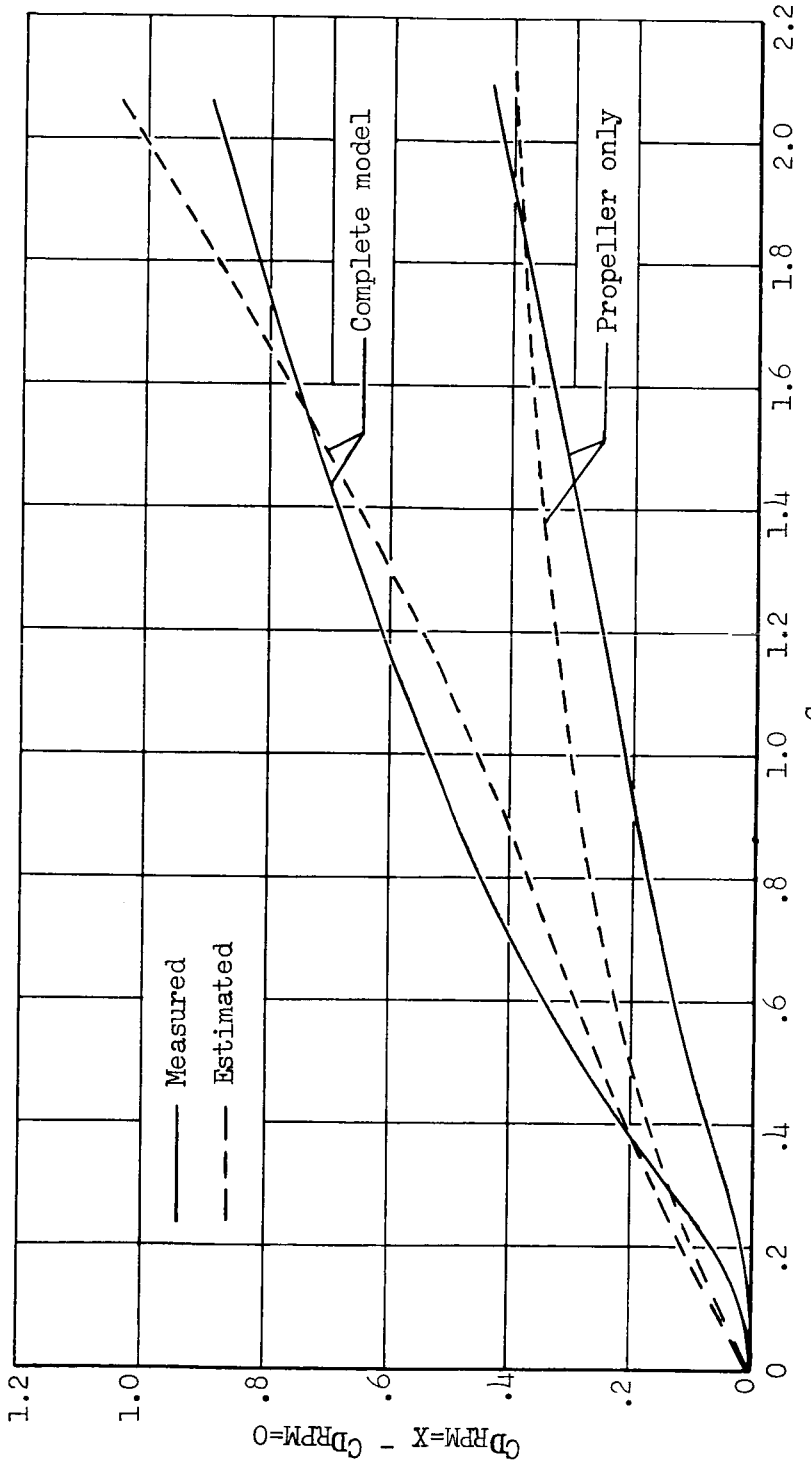

Figure 14.- Comparison of the estimated and measured variation of drag coefficient with propeller force coefficient; $\alpha = 0^{\circ}$, $\beta = 31^{\circ}$.

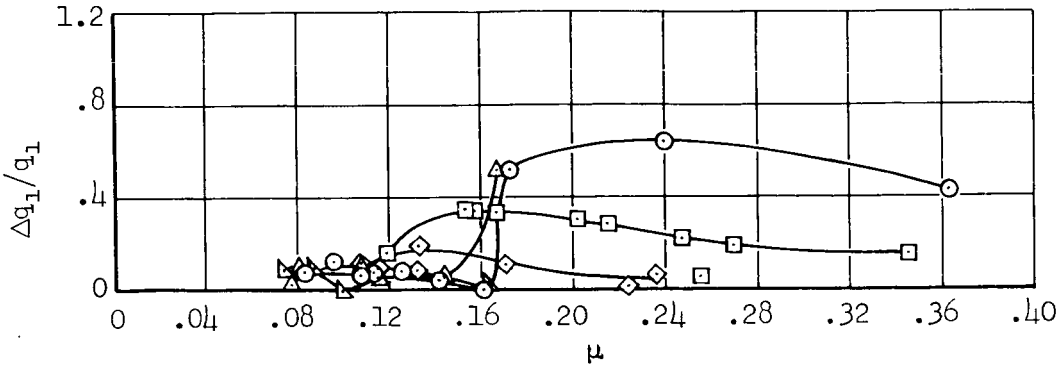

(a) Streamwise.

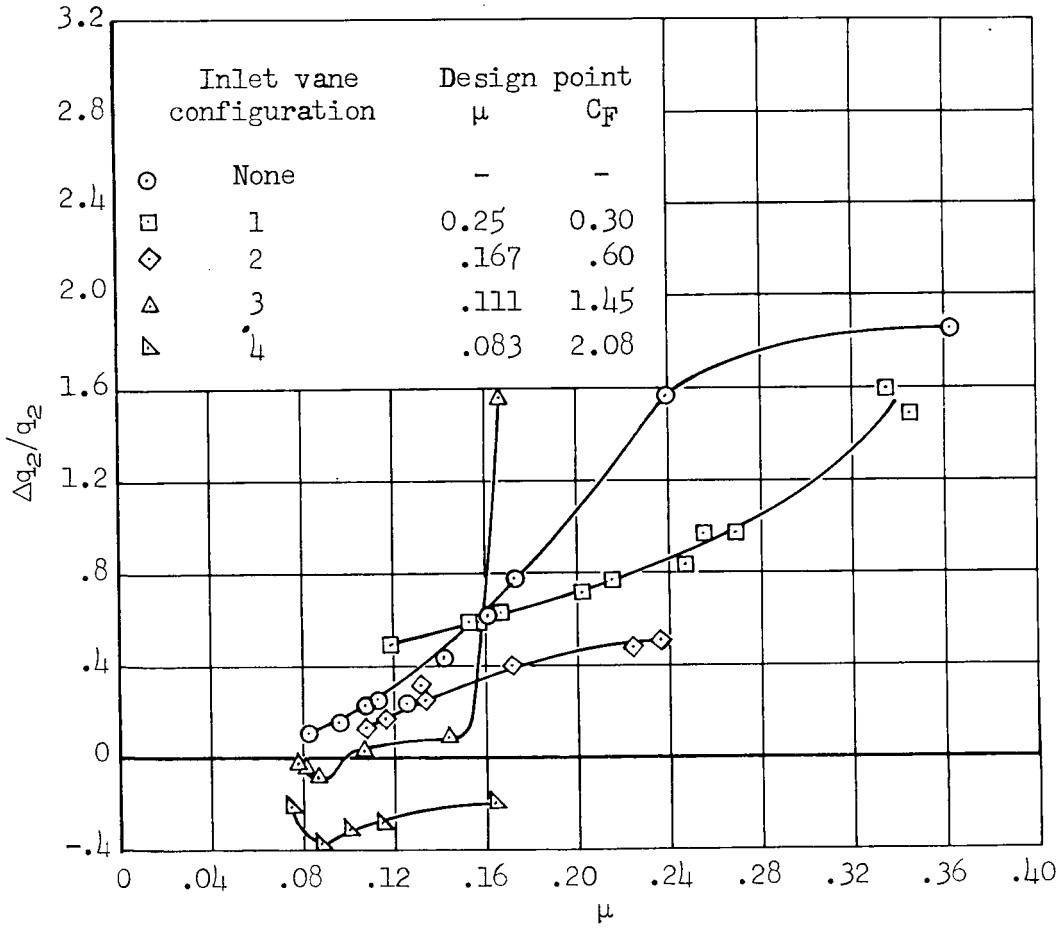

(b) Spanwise.

Figure 15.- Differential average wake dynamic pressures in terms of wake pressure with no forward speed at the same propeller rpm; $\alpha = 0^\circ$, $\beta = 31^\circ$.

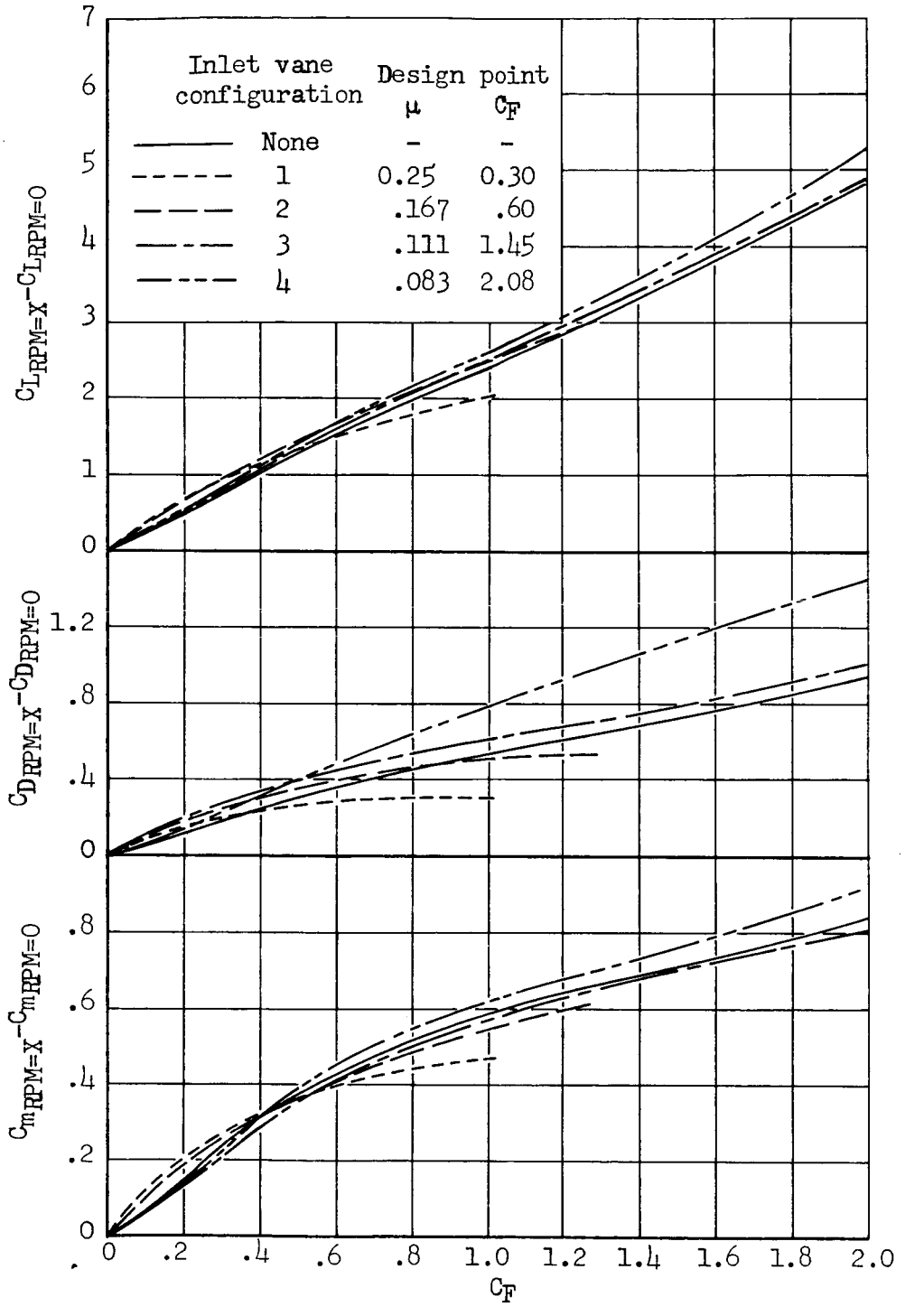

(a) Inlet vanes adjusted for unseparated flow at several values of C_F.

Figure 16.- The effect of inlet vanes on the variation of incremental complete-model force coefficients with propeller force coefficient; $\alpha = 0^\circ$, $\beta = 31^\circ$.

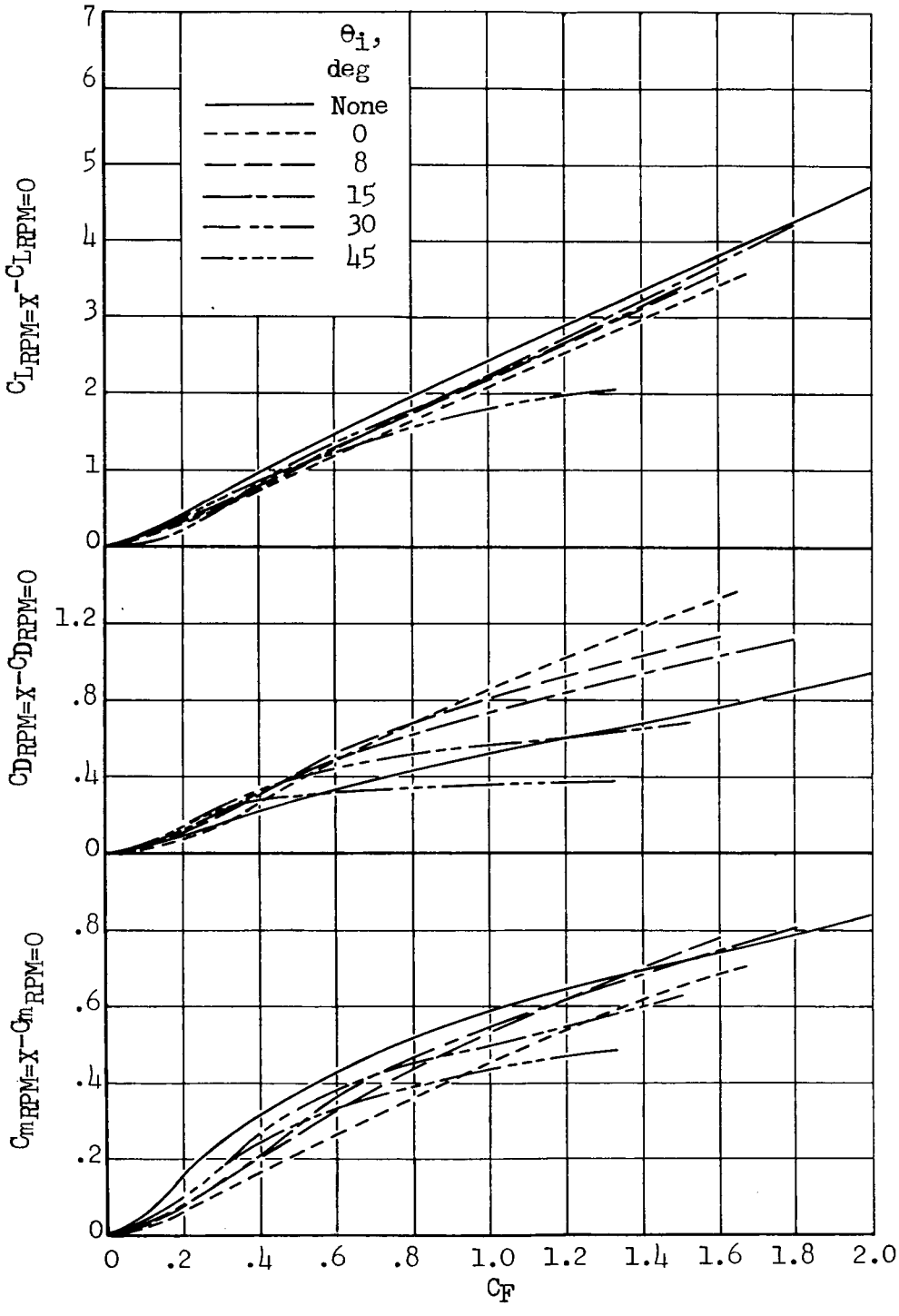

(b) All inlet vanes at the same angle.

Figure 16.- Concluded.

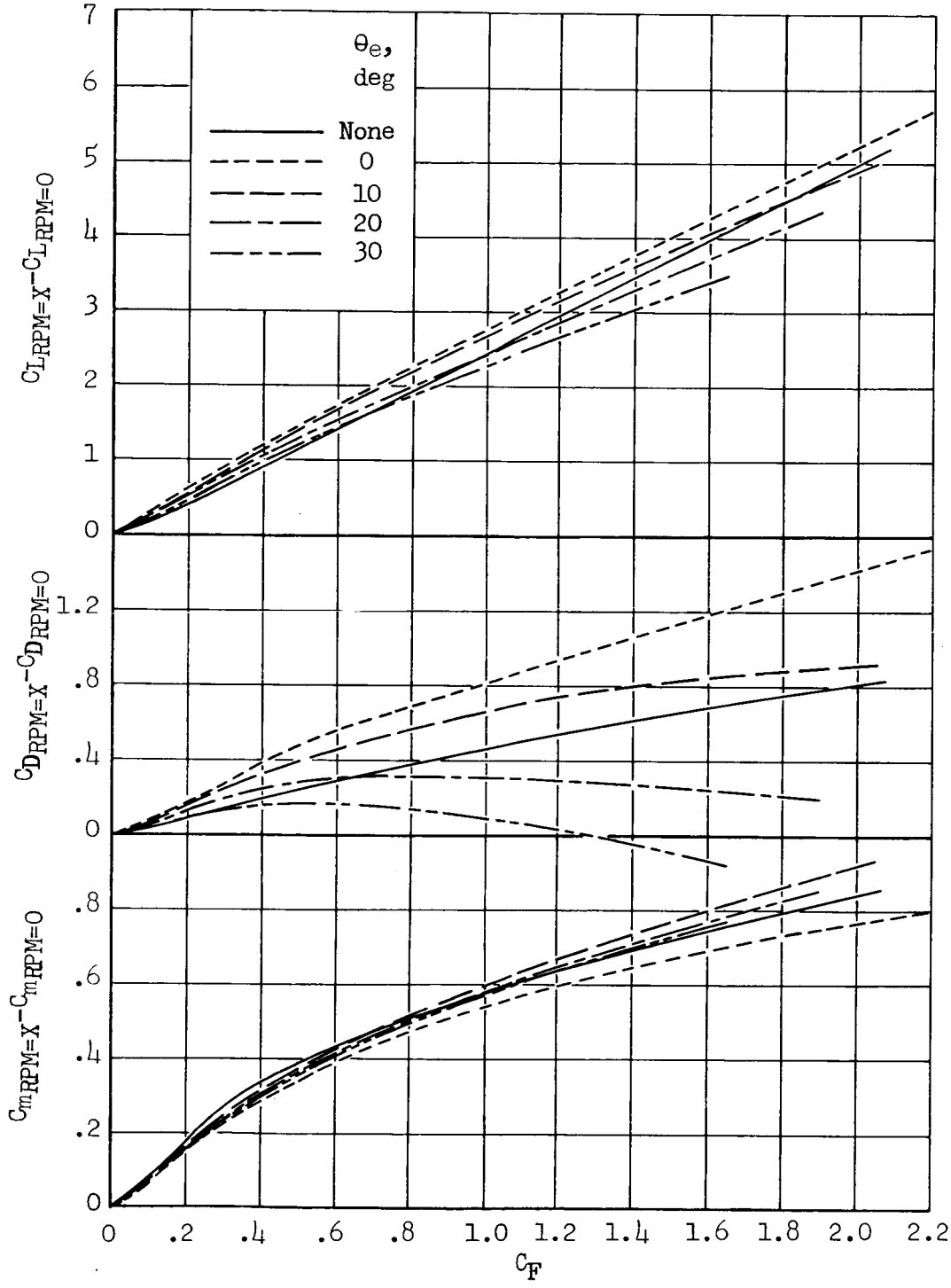

Figure 17.- The effect of duct exit vanes on the variation of complete-model incremental force coefficients with propeller force coefficient; $\alpha = 0^\circ$, $\beta = 31^\circ$.

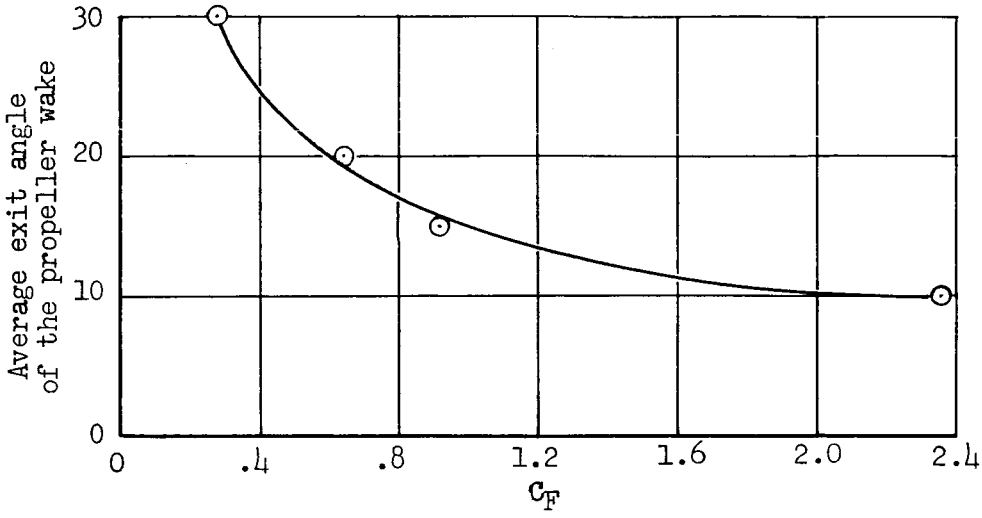

Figure 18.- Variation of the average wake exit angle with propeller loading; $\alpha = 0^\circ$, $\beta = 31^\circ$.

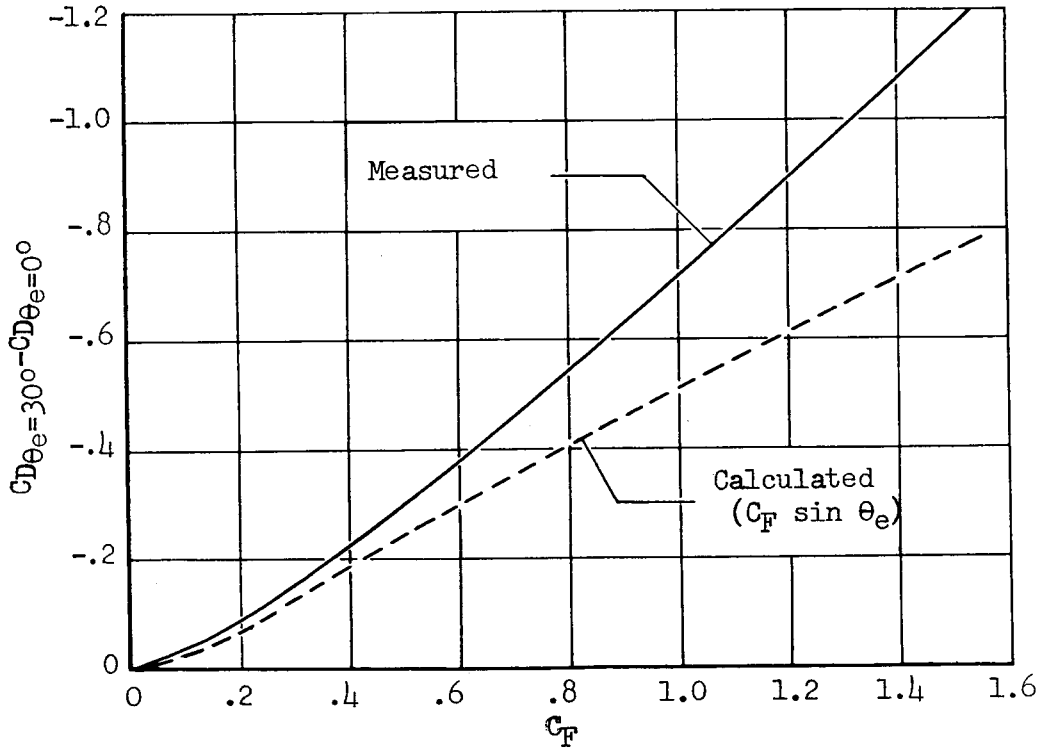

Figure 19.- Comparison of measured and estimated drag coefficient increments caused by redirecting the propeller wake 30° with exit vanes; $\alpha = 0^\circ$, $\beta = 31^\circ$.

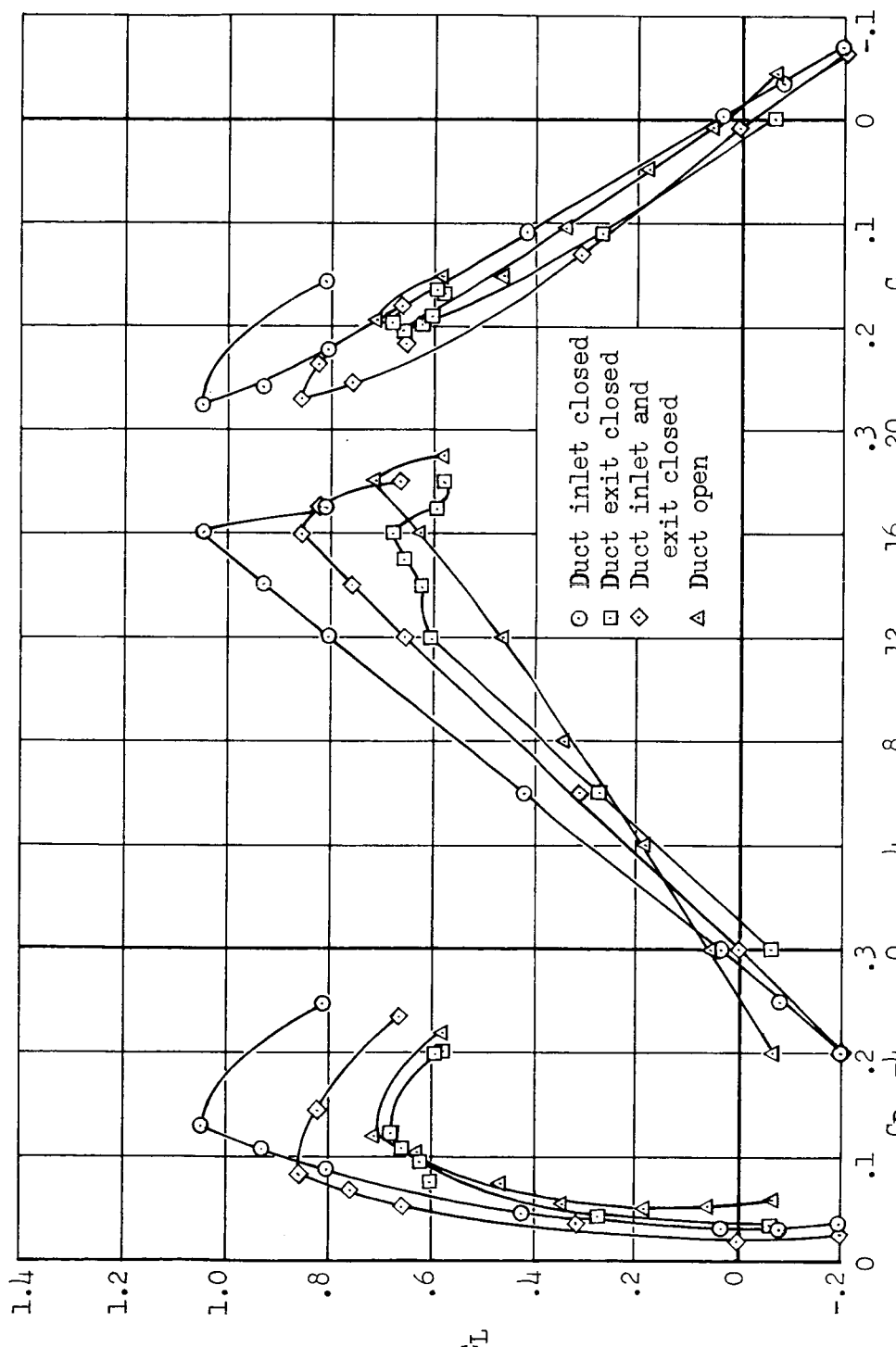

Figure 20.- Longitudinal characteristics of the model with the propeller and drive motor removed from the wind tunnel; Reynolds number = 1.4×10^6, q_∞ = 9 psf.

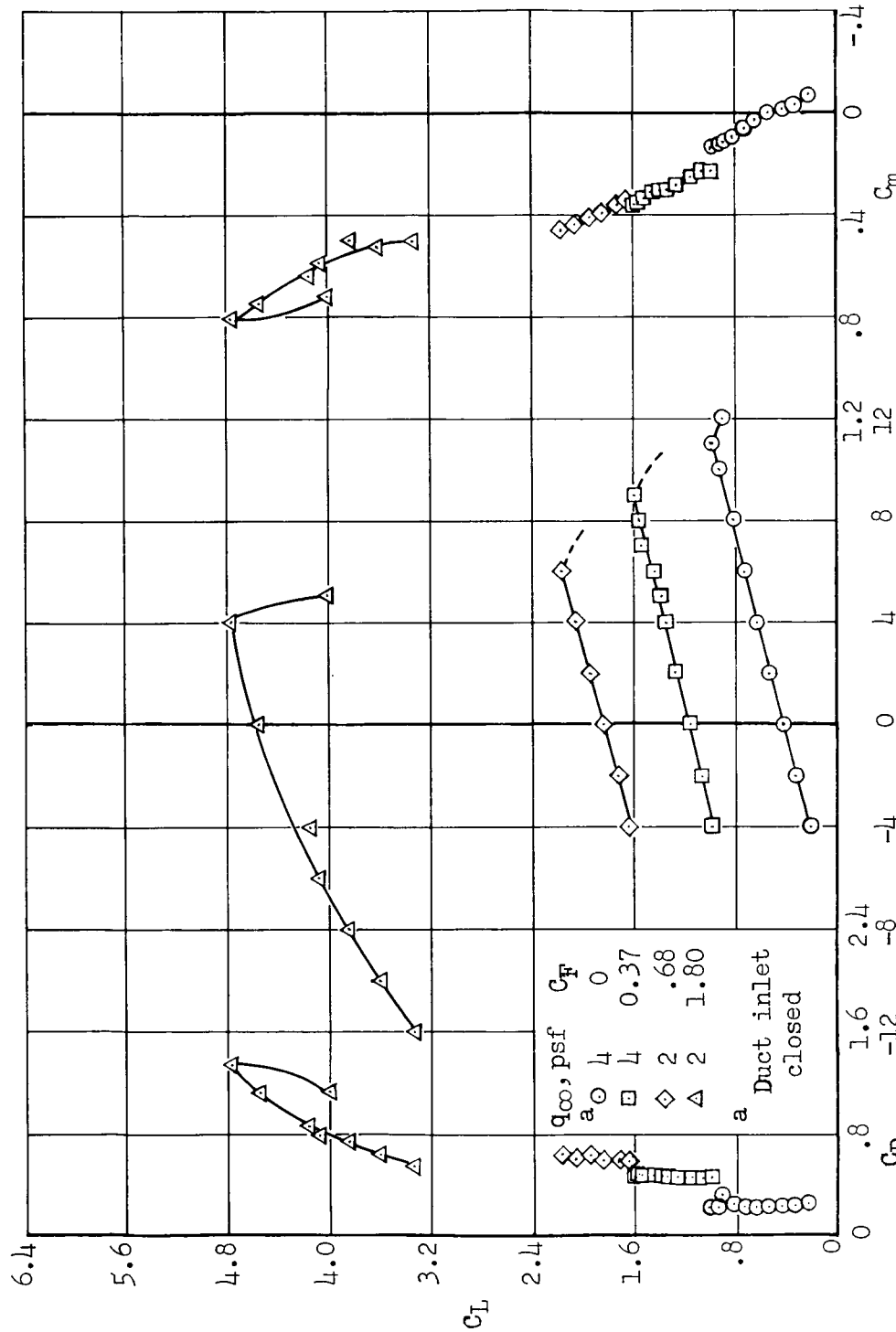

Figure 21.- Longitudinal characteristics with the propeller operating; $\beta = 31^\circ$.

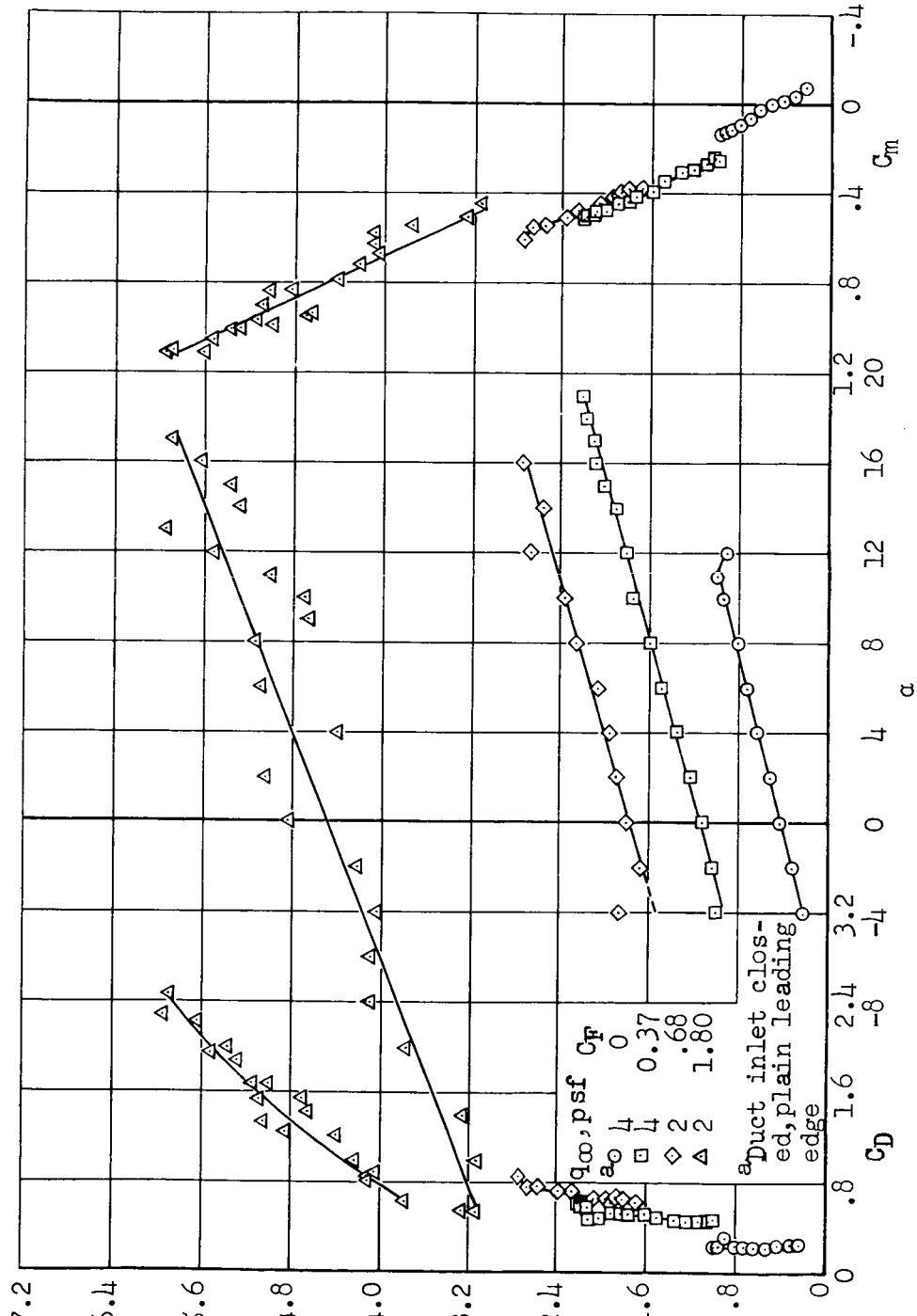

Figure 22.- Longitudinal characteristics of the model with the modified leading edge and the propeller operating; $\beta = 31^\circ$.

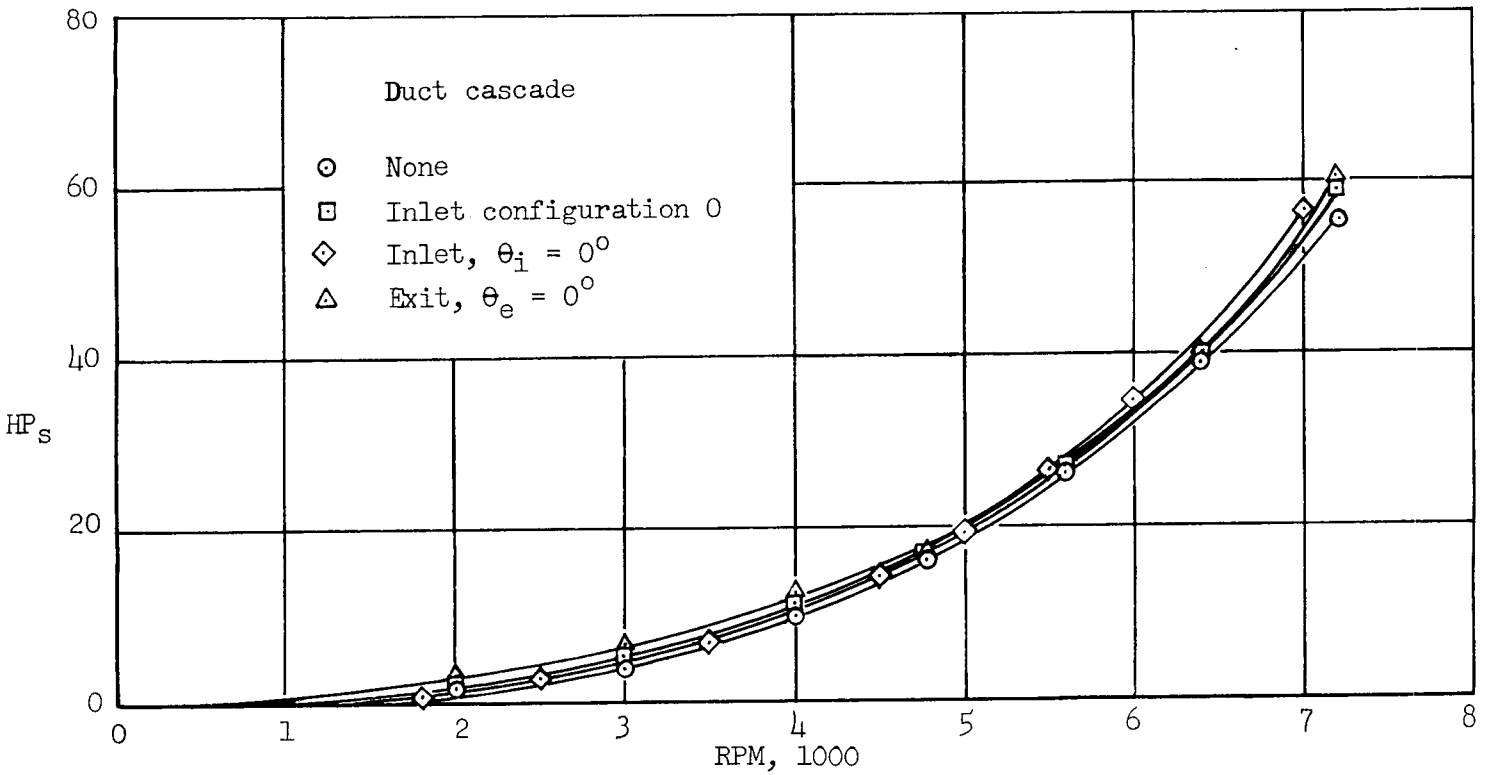

Figure 23.- Effect of the duct cascades on static power requirements; $\alpha = 0^o$, $\beta = 31^o$.

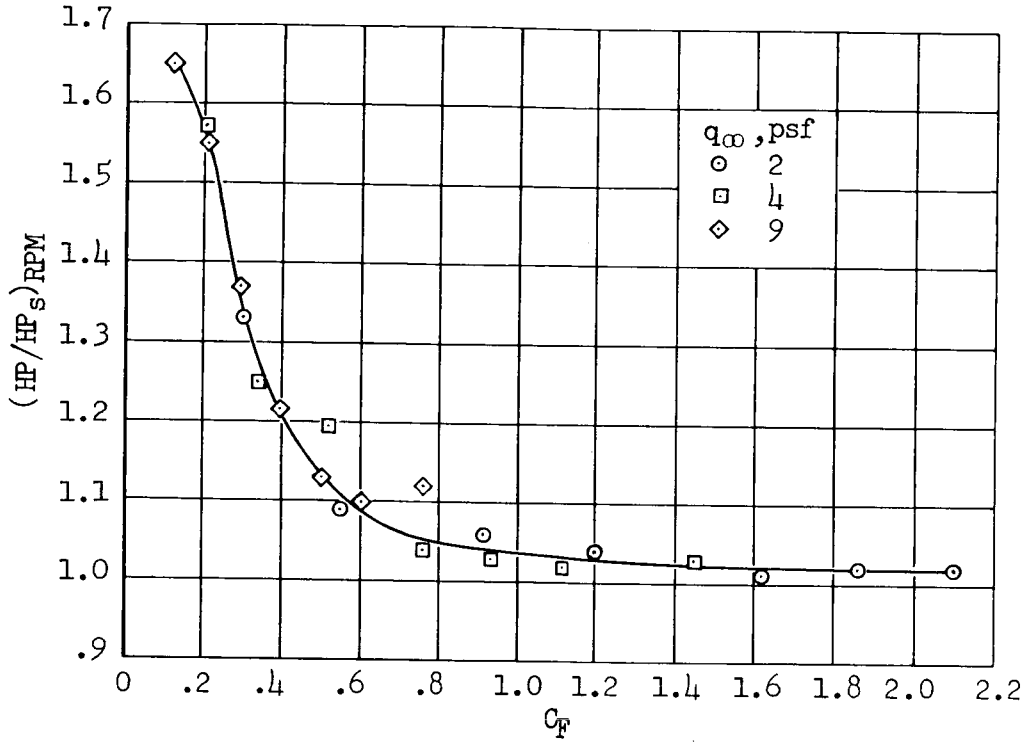

(a) Without a duct cascade.

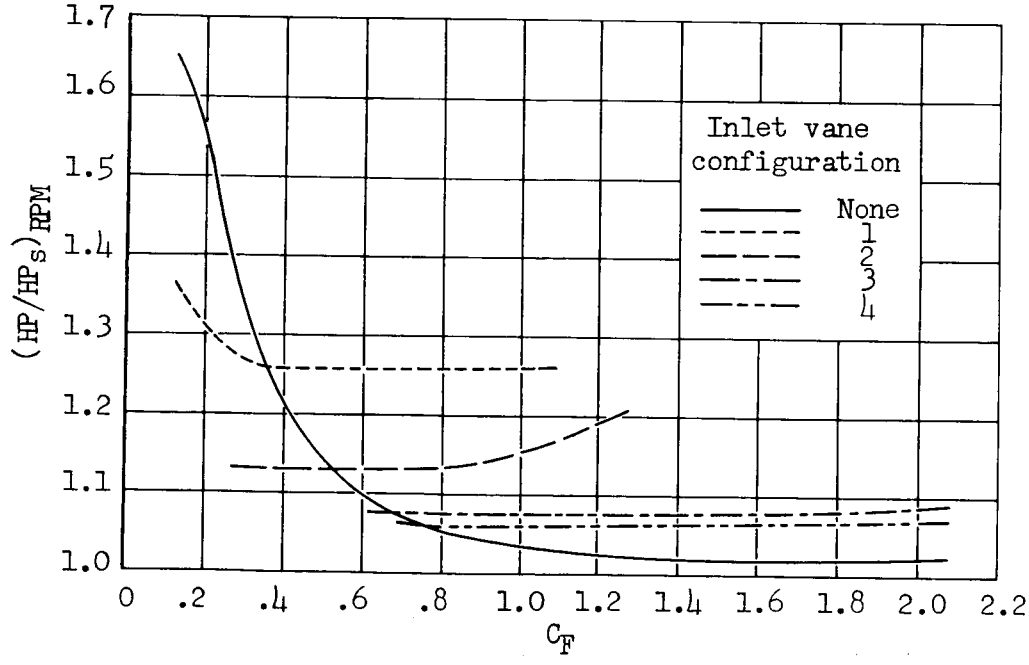

(b) With the inlet cascade.

Figure 24.- The variation with propeller force coefficient of the ratio of power at forward speed to static power with the same propeller rpm; $\alpha = 0^\circ$, $\beta = 31^\circ$.

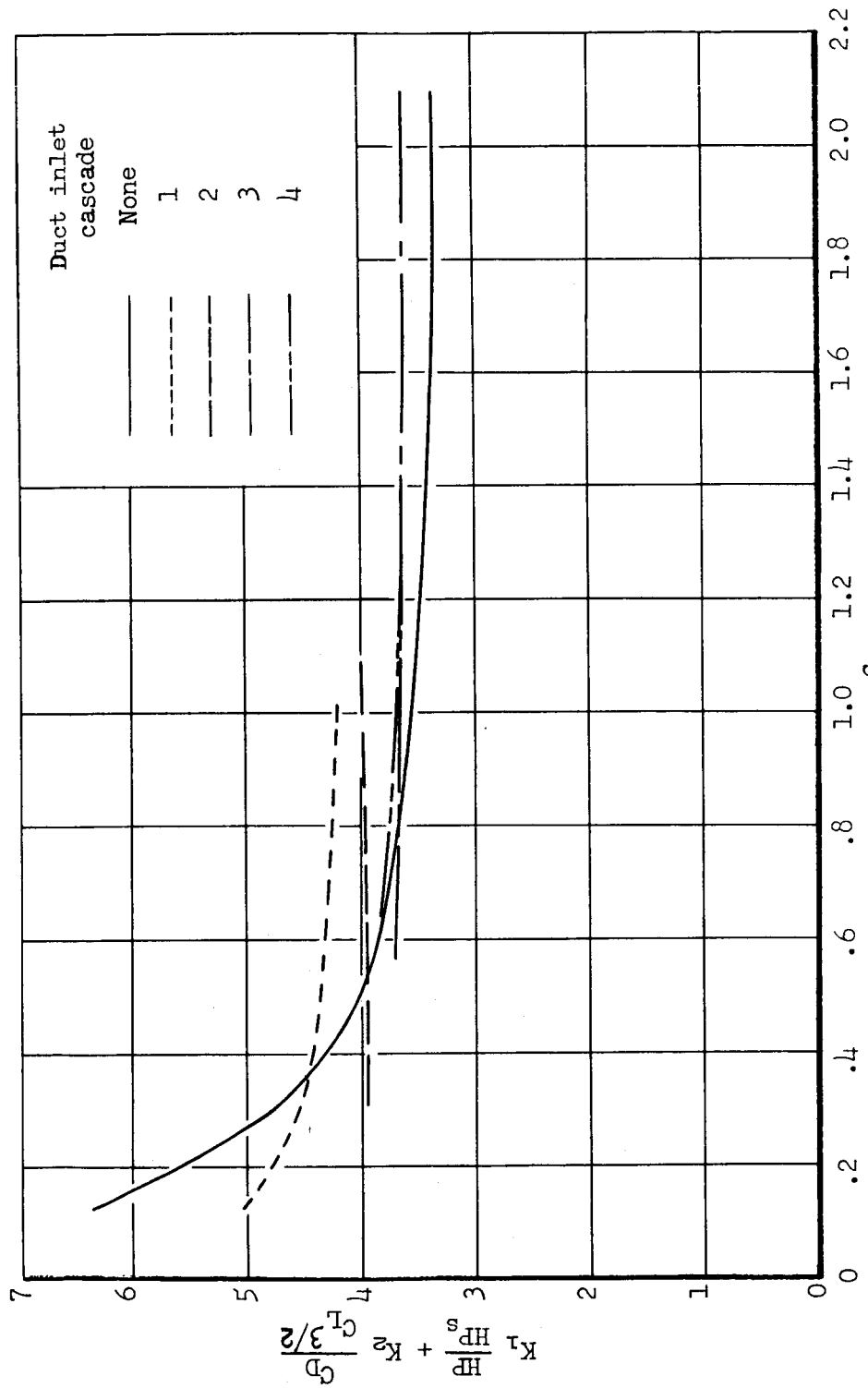

Figure 25.- Relative total horsepower required; $\alpha = 0^\circ$, $\beta = 31^\circ$.

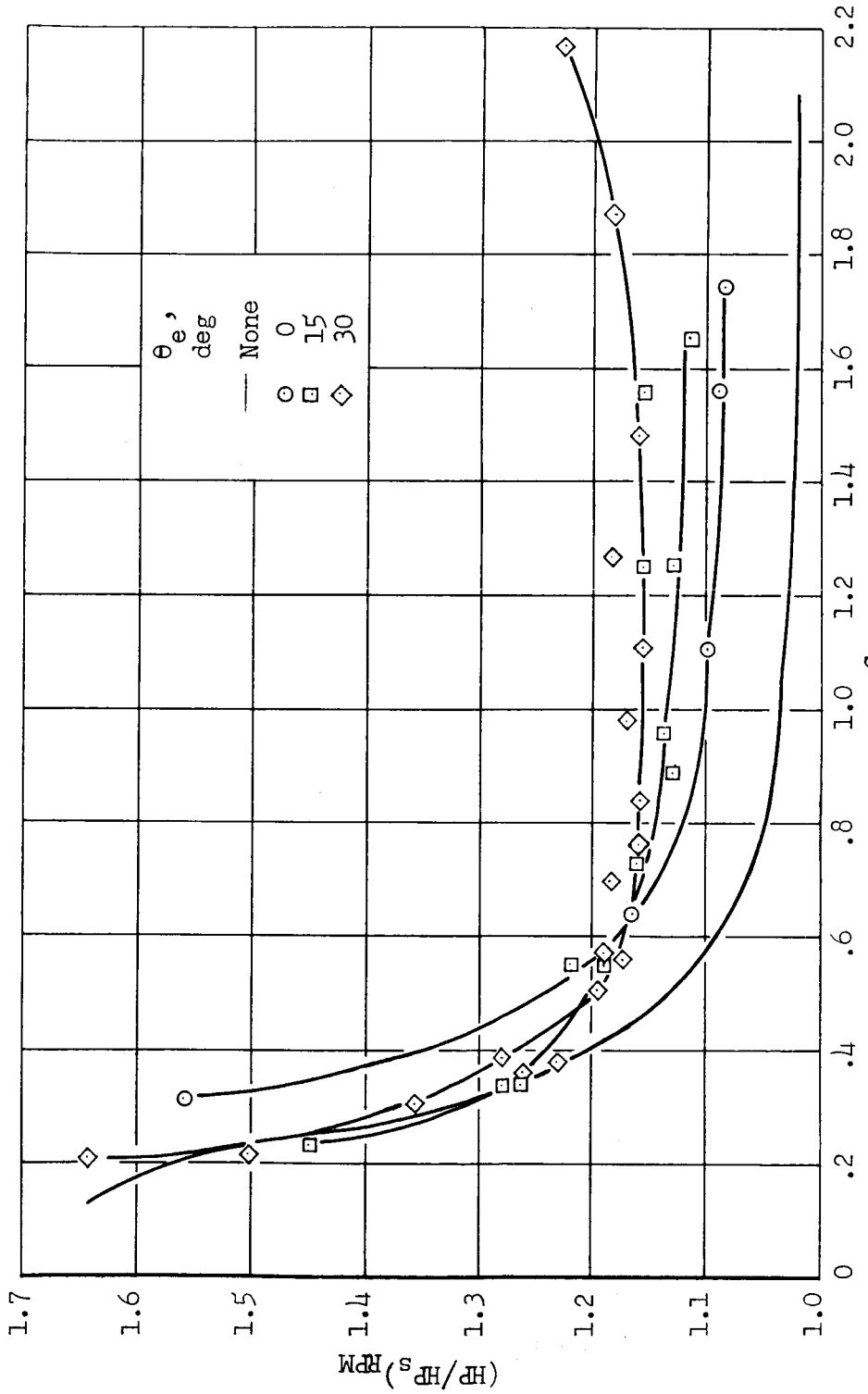

Figure 26.- The effect of the duct exit cascade on the ratio of power with forward speed to static power at the same propeller rpm; $\alpha = 0^o$, $\beta = 31^o$.

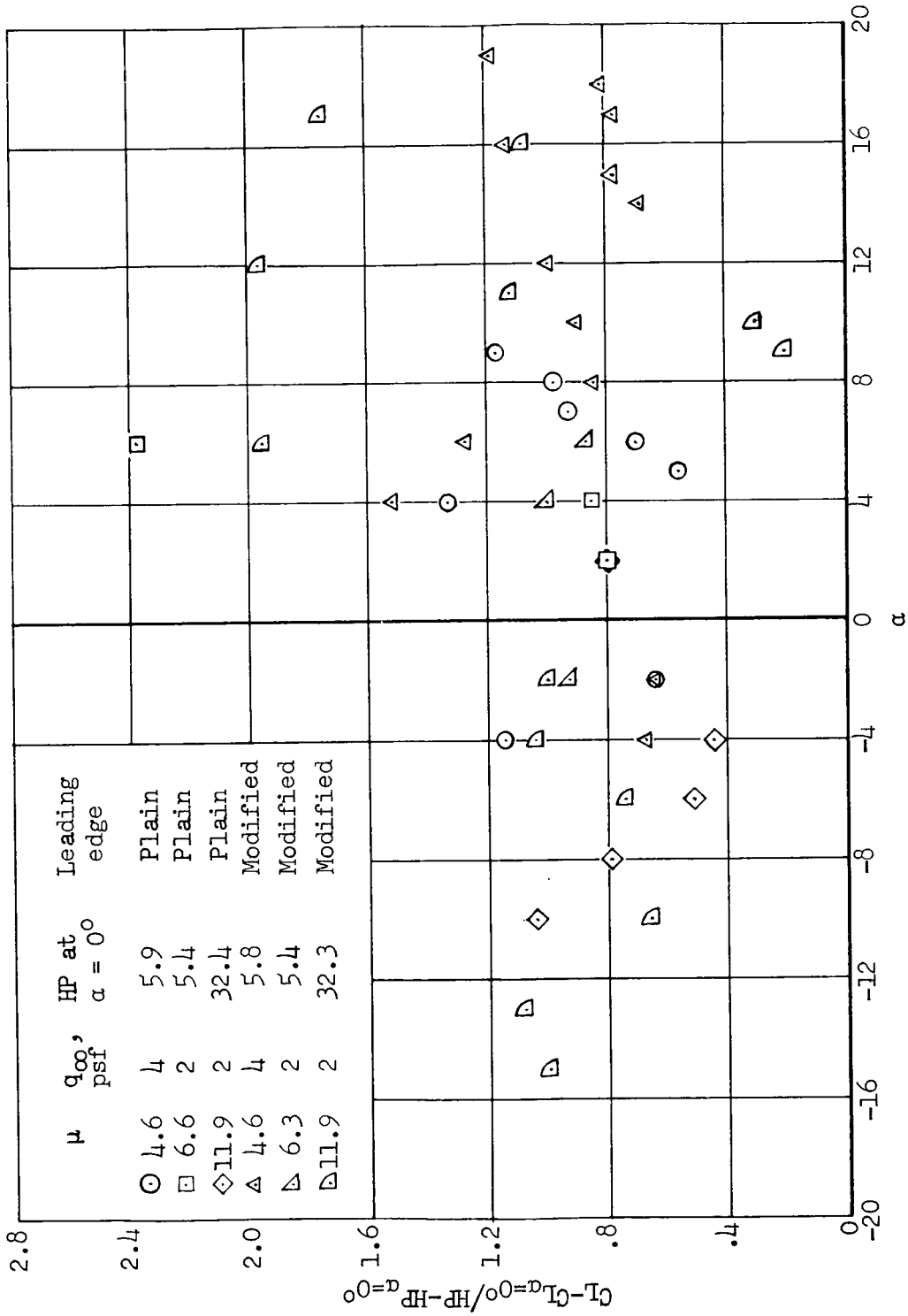

Figure 27.- The effect of angle of attack on the incremental ratio of lift to power; β = 31°.